

Modeling Cluster Production at the AGS

D. E. Kahana², S. H. Kahana¹, Y. Pang^{1,3},
 A. J. Baltz¹, C. B. Dover¹, E. Schnedermann¹,
 T. J. Schlagel^{1,2}

¹*Physics Department, Brookhaven National Laboratory
 Upton, NY 11973, USA*

²*Physics Department, State University of New York,
 Stony Brook, NY 11791, USA*

³*Physics Department, Columbia University,
 New York, NY 10027, USA*

(September 30, 2018)

Deuteron coalescence, during relativistic nucleus-nucleus collisions, is carried out in a model incorporating a minimal quantal treatment of the formation of the cluster from its individual nucleons by evaluating the overlap of initial cascading nucleon wave packets with the final deuteron wave function. In one approach the nucleon and deuteron center of mass wave packet sizes are estimated dynamically for each coalescing pair using its past light-cone history in the underlying cascade, a procedure which yields a parameter free determination of the cluster yield. A modified version employing a global estimate of the deuteron formation probability, is identical to a general implementation of the Wigner function formalism but can differ from the most frequent realisation of the latter. Comparison is made both with the extensive existing E802 data for Si+Au at 14.6 GeV/c and with the Wigner formalism. A globally consistent picture of the Si+Au measurements is achieved. In light of the deuteron's evident fragility, information obtained from this analysis may be useful in establishing freeze-out volumes and help in heralding the presence of high-density phenomena in a baryon-rich environment.

25.75, 24.10.Lx, 25.70.Pq

I. INTRODUCTION

Several coalescence models [1–11], have been proposed for calculation of cluster production in heavy ion collisions. In this paper we examine the use of such modeling for deuterons only, and with particular reference to existing Si+Au data at AGS energies. We demonstrate that it is necessary to understand something of the quantum mechanical aspects of coalescence in order to extract the absolute magnitude of cluster yields. Given this, it may then also be possible that information on the size of the ion-ion interaction region, complementary to that from HBT [12], will flow from a study of deuteron production. It must be emphasized that the interaction region or “fireball” spatial extent can only be gathered from knowledge of *absolute* deuteron yields and is in general lost if, for example, the acceptances for formation in position and momentum are adjusted to make theoretical yields agree with experiment [11,13] and/or the quantal aspects are ignored as in the “cutoff” models described in what follows. Most interesting would be the case of disagreement between an improved, self-consistent, cascade calculation and experiment. One would like to conclude, in the presence of such a discrepancy, that the fireball lives significantly longer (or shorter) than the cascade suggests. Our development can be usefully compared to a study by Koonin [14] of the nucleon pair correlation function generated in heavy ion collisions. The deuteron provides the best cluster for present purposes because, although the simplest, its spatial dimensions are still quite comparable to those expected for ion-ion interaction regions. The use of larger clusters may complicate the theory without adding much to use of coalescence as a probe of unusual medium effects. We emphasize that the rapidity region considered in this work, both theoretically and experimentally, avoids the target and projectile points where confusion with “boiled” off clusters might occur. Perhaps more importantly, the deuteron is weakly bound and its final materialization most likely occurs only after cessation of strong interactions for the coalescing nucleon pair. Thus a factorization of the calculation into a piece arising from the cascade, i.e. the pair nucleon distributions, and one arising from the quantum coalescence, is very probably a realistic description.

Since bound state formation is sensitive to the presence of even a slight correlation between the space-time and momentum vectors of the two coalescing nucleons, one can also extract from deuterons evidence for collective motion, i.e. hydrodynamic flow. The latter analysis may be complicated by the presence of "preformed" deuterons in both target and projectile regions of rapidity. We in fact examine the content of our produced deuterons to establish whether the two nucleons come from the same or different initial nuclei. A sizeable correction due to deuteron formation was indeed necessary for evaluating the level of nearly forward protons generated in Si+ Pb collisions at 14.6 GeV [16,17], wherein a very rudimentary version of coalescence was used. However, and not surprisingly, there is in the final analysis a strong, and useful, correlation between deuteron parentage and rapidity.

As noted, the weak binding of the deuteron can also be used to advantage, permitting one to factor production into an initial stage in which the event simulator, in this case ARC [15,16], generates the single nucleon distributions, and a second stage in which the coalescence takes place. The separation between these stages is reasonably well defined for the deuteron; it is marked by the last collision of both of the combining nucleons, i.e. at "freezeout". Earlier formation, or at least survival, of the weakly bound deuteron is unlikely. It is in just such circumstances that the more global coalescence models can be best expected to work. Just what one means by "last" collision is, however, also subjected to some scrutiny here. The simulation is cut off below some cm energy for colliding (not coalescing) particles, and the sensitivity to this cutoff is tested. One might comment at this point that coalescence of anti-deuterons in ion collisions should be very similar to that of deuterons. The anti-nucleon and nucleon distributions might differ appreciably, the anti-particles being in some senses surface-constrained by annihilation [18], but the freezeout of anti-deuterons is again dominated by the low binding energy. We will examine such exotic clusters in future work, although we include some discussion here.

Another advantage of weak deuteron binding is that more "microscopic" but harder processes, such as concomitant final state π production, are considerably less likely than the soft coalescence. Given anticipated limitations on the level of accuracy in both data and our present theory, we ignore these auxiliary channels.

The coalescence model depends crucially on the space and momentum distributions of neutrons and protons. To be as precise as possible we use the relativistic cascade ARC [15,16], which has been very successful in describing and predicting [19] the measured nucleon spectra in several AGS experiments. As we will show in Sec. 3, the interface between the ARC code and the coalescence model is relatively simple, but still requires some design choices.

Another important ingredient is the quantum mechanical "device" used to marry the ARC distributions to the bound wave function. Ideally this would be done at the microscopic level, with perhaps interaction with a "field" or a third object placing the deuteron on-shell. We will, for obvious reasons, stick with the coalescence model. We will in fact perform three related calculations to test the quantal and spatial features of the coalescence modeling:

- Static: A calculation in which neutron, proton and deuteron wave packet sizes are set externally and globally.
- Dynamic: A calculation in which the sizes are determined for each coalescing pair during the cascade.
- Wigner: A calculation using the Wigner function formalism. We consider two variants:
 - (1) Wigner as generally implemented (Standard Wigner).
 - (2) Wigner as introduced below (Quantal Wigner).

Our standard calculation, referred to hence as ARC Dynamic, is the second of these because of its physical basis and because it alone yields the possibility of a parameter free determination of absolute deuteron yields. The Wigner characterisation should itself be divided into two limiting cases, discussed in some detail in what follows. A "generalized" Wigner procedure is precisely equivalent to the first or Static wave packet scheme. Once one has factorized the calculation into two parts, the overlap integral estimating deuteron formation may be subjected to the Wigner transformation. The result is a convolution of the deuteron Wigner transform with the neutron and proton Wigner functions. An "exact" Wigner simulation would then assign wave packets to the two nucleons, taking account of the central or average position and momenta of these packets. If for example one selects some appropriate smearing size for the single particle wave functions and performs the requisite convolution with the known bound-state deuteron Wigner function, then the Wigner procedure is identical to the Static approach, both incorporating the quantum mechanics inherent in the overlap integral.

However in the "standard" Wigner treatment, generally employed [3,7,9], one attempts to fix both the (classical) momentum and position of cascading particles, a procedure at variance with the precepts of quantum mechanics. This constitutes a definite approximation to the quantal treatments presented above. One might very well wish to compare the results of this Standard Wigner, with apparently no quantal smearing specified for the initial nucleons, with those of the generalised Wigner with some smearing $\sim 1fm$. We compare these approaches with each other and with Dynamic coalescence. This comparison (see Figs. 5,6) exhibits appreciable disagreement in absolute deuteron yields, with interestingly the largest divergence between the two Wigner calculations.

Our results are predicated on the factorisation referred to above, i.e. coalescence should occur only after all reactions have ceased for the participant np pair. We require then a knowledge of both the relative distance of the two nucleons *and of* the spatial extent of their wave packets at the freeze-out time of each pair. The distribution of the former is assumed given by the cascade; the latter ostensibly follows from the quantum mechanical history of the individual nucleons somewhat before and during coalescence. Fortunately, deuteron formation seems to be sensitive only to the size of the packets and not to finer details.

The internal deuteron wave function is well known [20,21]. We demonstrate below that only moderate sensitivity exists to the root mean square radius r_d of the deuteron and hence we do not expect great dependence on the specific form of wave function. We test this sensitivity by using as a measure of the deuteron bound state size both the charge radius determined from electron scattering and the “point” radius obtained after removing the finite proton charge radius. In Static the wave packet sizes are externally fixed, remaining the same for an entire nucleus-nucleus collision. For Dynamic the wave packet sizes are determined separately from the environment of each pair. Causality suggests that a given nucleon should be affected only by hadrons in its past light cone. This will be kept in mind when determining the wave packets of a coalescing pair. The potentially new element that wish to highlight is the physics represented by the parameter(s) describing the spatial extent of the nucleon wave packets. These parameters, largely ignored in earlier calculations or hidden in the choice of Wigner function, should perhaps be related to the size of the interaction region generating or “preparing” the single nucleon distributions [14]. One might have imagined the Wigner formalism would be tied to the use of a small wave packet size or smearing. Figures 3 and 4 would seem to suggest otherwise.

In earlier work [11] we considered the formation of a weakly bound (1-15 MeV) $\Lambda\Lambda$, our version of the H-dibaryon. There, however, a coalescence prescription was used confining bound state production to baryon pairs contained within a certain region in the relative six-dimensional phase space. The radii of this allowed region were related to the relative position and momentum content of the true (but unknown) H wave function. The normalisation for the di-hyperon cross-section was obtained, however, by comparing a similar cutoff calculation for the deuteron to existing data [24]. It is such a cutoff model that we intend to improve on here.

Section 2 contains a rudimentary coalescence theory, including a brief statement of the relation between the wave packet and Wigner approaches. Section 3 describes implementation of our preferred approach, ARC Dynamic, within the framework of ARC, and in Section 4 we examine our results with an eye to understanding the quantal effects introduced above and to comparing these results to published measurements [24]. In general the dynamical approach does surprisingly well in reproducing the overall experimental Si+Au measurements, both detailed transverse-mass spectra and significantly, the absolute magnitudes. The confidence generated by this result encourages us to pursue the matter further, to the point of suggesting that unexpected measured deuteron production might signal unusual behaviour.

Section 5 contains highly instructive details of the space-time and momentum evolution of coalescing pairs within the Dynamic simulation which can lead to some estimates of freezeout sizes at the time of coalescence. Section 6 contains a brief summary. One must keep in mind that to at least some extent the success of the cascades, in general and in their treatment of cluster formation, depends on the considerable degree of averaging taking place even in a single ion-ion event. Nevertheless, the theory produces a credible picture of the physics, as will become clear in what follows.

II. COALESCENCE THEORY

A. Overlap Ansatz

The “bare-bones” coalescence model first proposed historically [2], was one in which only the relative momentum of combining particles need be within a predetermined range. Strictly speaking, such a limit is only valid if the particle source is small in comparison to the final bound state. Effectively, one is then using plane waves for the single particle wave packets. In its simplest incarnation the coalescence model forms a deuteron from a proton and a neutron if their relative momenta are within a certain *capture radius* p_0 , comparable to the deuteron’s momentum content. The deuteron cross section can then be computed (non-relativistically) in terms of the proton and neutron cross sections as

$$\frac{d\sigma_d}{dp^3}(\mathbf{p}) = \frac{3}{4} \frac{4\pi p_0^3}{3} \frac{d\sigma_p}{dp^3}\left(\frac{\mathbf{p}}{2}\right) \frac{d\sigma_n}{dp^3}\left(\frac{\mathbf{p}}{2}\right) \quad (1)$$

where $\frac{3}{4}$ is the combinatoric factor for angular momentum [5,7].

For pA collisions the omission of any spatial dependence is perhaps justified, given that the interaction region is small enough for both deuteron wave function and nucleon density to be taken constant. For ion-ion collisions the final interaction region might in fact include the entire smaller nucleus and some account must be taken of spatial dimensions relative to the deuteron. Consequently, the momentum capture radius p_0 , as extracted from measured proton and deuteron spectra, exhibits an unnatural variation with target and projectile [22,23]. We are attempting to elaborate upon this observation here.

In examining the H-dibaryon and deuteron formation in ion collisions [11], the present authors extended this ‘‘cutoff’’ coalescence to include a constraint on both relative spatial and momentum separations of combining baryons, i.e. one then defined an allowed six, rather than three-dimensional phase space region. By normalising to measured deuteron yields in Si+Au collisions, we hoped to remove ambiguities in the H-yield. These cutoff calculations can not determine absolute cluster magnitudes, incorporating as they do a strong dependence on the six-dimensional phase-space volume in which coalescence takes place. The finite size of the deuteron may presage an interesting dependence of production on impact parameter, over and above that due to the single nucleon distributions.

The naive-cutoff coalescence prescriptions have major shortcomings. In the first instance the purely momentum treatment contains no spatial information, while the extended space-momentum version introduces such information in an ad hoc fashion. This cannot be easily fixed without violating quantum mechanics which evidently forbids the simultaneous use of precise momentum and space coordinates. Further, since the quantum mechanics of the formation is absent, so is the actual deuteron wave function, which might perhaps be of essential importance in the microscopic process. These shortcomings can be avoided within a rudimentary quantum mechanical model [7,9,10,14] which assumes that neutron and proton are described by wave packets of width σ localized in space around $\bar{\mathbf{x}}_i$ and in momentum space around $\bar{\mathbf{p}}_i$:

$$\psi_i(\mathbf{x}) = \frac{1}{(\pi\sigma^2)^{3/4}} \exp\left(-\frac{(\mathbf{x} - \bar{\mathbf{x}}_i)^2}{2\sigma_i^2}\right) \exp\left(i\bar{\mathbf{p}}_i \cdot \mathbf{x}\right) \quad (2)$$

The two ARC approaches, Dynamic and Static are distinguished at this point by choice of the size parameters σ_i for the neutron and proton. In the latter this choice is simple, a single global value for all pairs and events. It is surely a simplification to imagine one spatial parameter describes all nucleons partaking in an ion-ion collision. However, considering the complexity of the interactions a reasonable averaging may result. The determination of σ for Dynamic coalescence from the pair history is described in the next section.

We write the deuteron wave function as a product of its center-of-mass motion and its internal motion

$$\psi_d(\mathbf{x}_1, \mathbf{x}_2) = \Phi_{\bar{\mathbf{P}}, \bar{\mathbf{R}}}(\mathbf{R}) \phi_d(\mathbf{r}) \quad (3)$$

where

$$\Phi_{\bar{\mathbf{P}}, \bar{\mathbf{R}}}(\mathbf{R}) = \frac{1}{(\pi\Sigma^2)^{3/4}} \exp\left(-\frac{(\mathbf{R} - \bar{\mathbf{R}})^2}{2\Sigma^2}\right) \exp\left(i\bar{\mathbf{P}} \cdot \mathbf{R}\right) \quad (4)$$

and

$$\phi_d(\mathbf{r}) = (\pi\alpha^2)^{-3/4} \exp(-r^2/2\alpha^2) \quad (5)$$

In the above $\mathbf{R} = \frac{1}{2}(\mathbf{x}_1 + \mathbf{x}_2)$ and $\mathbf{r} = \mathbf{x}_1 - \mathbf{x}_2$, and we have allowed for, but do not exploit, the possibility that the deuteron center of mass and initial neutron(proton) wave packets are described by different size parameters. A natural assumption, which we will make here for simplicity, is that during coalescence the two body cm motion is unaltered, leading to $2\Sigma^2 = \sigma^2$. In fact it is a rather gentle interaction with some third particle which puts the deuteron on shell and some small dependence on the center of mass coordinates should remain. Given that the deuteron is weakly bound, we assume the latter is small.

We could improve on the choice of relative wave function for the deuteron, reducing the transparency of the calculation somewhat. For reasonably central collisions with massive nuclei the single gaussian should be adequate, especially in light of the other simplifications being made. For the most extreme peripheral collisions, where the fireball size might rival or be even less than that of the deuteron, this might cause a problem. One could test this point with an improved wave function, most easily by fitting several gaussian terms to say an existing deuteron wave function [20]. The question, here, is whether or not the coalescence is sensitive to higher moments of the relative motion, and not just to the rms radius. Probably, in view of the limitations of our modeling and the wholesale averaging in the ion-ion collision, such fine points are not significant. We test the sensitivity by varying the deuteron radius parameter somewhat, and find little effect (see Figs. 11,12).

The coalescence probability, or deuteron content of the two particle wave function, can now be computed from the squared overlap

$$C(\mathbf{x}_n, \mathbf{k}_n; \mathbf{x}_p, \mathbf{k}_p) = |\langle \psi_n \psi_p | \Phi_{\bar{\mathbf{P}}, \bar{\mathbf{R}}} \phi_d \rangle|^2. \quad (6)$$

With gaussian packets throughout this yields:

$$|\langle \psi_n \psi_p | \Phi_{\bar{\mathbf{P}}, \bar{\mathbf{R}}} \phi_d \rangle|^2 = \left(\frac{4\nu}{\sqrt{2\mu}} \right)^3 \exp\left(-\frac{\nu^2(\mathbf{k}_n - \mathbf{k}_p)^2}{2}\right) \exp\left(-\frac{(\mathbf{x}_n - \mathbf{x}_p)^2}{\mu^2}\right), \quad (7)$$

where $\mu^2 = (2\sigma^2 + \alpha^2)$, and $\nu = \frac{\alpha\sigma}{\mu}$.

We now assume that the (classical) distribution functions f_p and f_n of protons and neutrons, in so far as they can be obtained from a classical cascade, actually describe distributions of wave packets centered at the cascade particle positions and with momenta necessarily spread about the cascade values. Again, the choice of size parameters σ_i , $i = p, n, D$, for the wave packets is handled differently in our two protocols, uniformly for all coalescing pairs in one ion-ion event for Static and from the history of each pair for Dynamic. Including a factor of $\frac{3}{4}$ for spin the number of deuterons, and neglecting pairs lost to higher clustering, the deuteron number is then

$$n_d = \frac{3}{4} \int d\bar{\mathbf{x}}_n d\bar{\mathbf{k}}_n f_n(\bar{\mathbf{x}}_n, \bar{\mathbf{k}}_n) \int d\bar{\mathbf{x}}_p d\bar{\mathbf{k}}_p f_p(\bar{\mathbf{x}}_p, \bar{\mathbf{k}}_p) C(\mathbf{x}_n, \bar{\mathbf{k}}_n; \bar{\mathbf{x}}_p, \bar{\mathbf{k}}_p), \quad (8)$$

which, given the above interpretation of cascade distributions, may be written

$$n_d = \frac{3}{4} \sum_{ij} C(\mathbf{x}_{n_i}, \mathbf{k}_{n_i}; \mathbf{x}_{p_j}, \mathbf{k}_{p_j}), \quad (9)$$

with the sum extending over all appropriate pairs ij in the cascade. The quantum fluctuations of individual nucleons or of the deuteron center of mass motion are built in through the wave packets. The situation is different as we will see for the ‘‘Standard’’ application of the Wigner formalism, but not necessarily in a more straightforward realisation of the latter.

It should be noted, in agreement with References 5 and 7, that there is no isospin factor of one-half in this expression [13]; neutrons and protons can indeed be treated as distinguishable. If one were to use an isospin formalism it would be necessary to symmetrize the cascade input to coalescence with respect to the np pair, and the result inevitably is the same with the apparent factor of one-half compensated by a symmetry factor of two. The symmetrisation must be imposed externally since the classical cascade would never yield both $n(k_1)p(k_2)$ and $n(k_2)p(k_1)$.

B. Equivalence to Wigner Function Formalism.

The equivalence of the Wigner [7,9] and overlap coalescence is self evident under a factorization hypothesis, i.e. if one separates the cascade generation of single nucleon distributions from deuteron formation. One can re-express Eq. (8) for the deuteron yield in terms of Wigner functions f_i^W for the initial neutron, proton and final deuteron:

$$n_d^W = \frac{3}{4} \int d\mathbf{x}_1 d\mathbf{p}_1 f_p^W(\mathbf{x}_1, \mathbf{p}_1) \int d\mathbf{x}_2 d\mathbf{p}_2 f_n^W(\mathbf{x}_2, \mathbf{p}_2) f_{deut}^W(\mathbf{x}_1, \mathbf{p}_1; \mathbf{x}_2, \mathbf{p}_2). \quad (10)$$

These functions f_i^W are simply transforms of appropriate density matrices, in the fashion:

$$f_i^W(\mathbf{x}, \mathbf{p}) = \int d\boldsymbol{\eta} \rho_i(\mathbf{x} - \frac{\boldsymbol{\eta}}{2}, \mathbf{x} + \frac{\boldsymbol{\eta}}{2}) \exp(-i\mathbf{p} \cdot \boldsymbol{\eta}). \quad (11)$$

For pure states we may write the density distributions in terms of our previous wave functions as

$$\rho_i(\mathbf{x}, \bar{\mathbf{x}}) = \Psi_i(\mathbf{x}) \Psi_i^*(\bar{\mathbf{x}}). \quad (12)$$

Inserting the densities in Eq. (12) into Eqs. (10,11) and performing the required integrations results in

$$n_d^W = \sum_{ij} |\langle \psi_n \psi_p | \Phi_{\mathbf{P}, \mathbf{R}} \phi_d \rangle|^2, \quad (13)$$

which in fact implies the identity

$$n_d^W = n_d \quad (14)$$

provided only that the wave functions entering the Wigner transforms are the same as used in Eqs. (2,3). This comes as no surprise; the exact Wigner transformation in Eqs. (11,12) has been undone by inserting the density operators defined through wave packets into Eq. (10).

Standard Wigner [3,7,9] takes another path, specifying the neutron and proton distributions in Eq. (10) through

$$f_i^W(\mathbf{x}, \mathbf{k}) = \delta(\mathbf{x} - \mathbf{x}_i)\delta(\mathbf{k} - \mathbf{k}_i). \quad (15)$$

The treatments thus diverge when one uses this usual, but quantally disallowed, assumption for the Wigner distributions. In fact, in the case of a gaussian wave function for the bound deuteron, one can continue to use Eq. (9) with the Standard Wigner coalescence with

$$C(\mathbf{x}_{n_i}, \mathbf{k}_{n_i}; \mathbf{x}_{p_j}, \mathbf{k}_{p_j}) = 8 \exp(-\alpha^2(\mathbf{k}_{n_i} - \mathbf{k}_{p_j})^2) \exp\left(-\frac{(\mathbf{x}_{n_i} - \mathbf{x}_{p_j})^2}{\alpha^2}\right), \quad (16)$$

where α is the deuteron size parameter, related to the “point” rms radius r_P by

$$(r_P)^2 = \frac{3}{2}\alpha^2 \quad (17)$$

There are evidently no free parameters in this result, any smearing of the nucleon positions and momenta is hidden and perhaps arises only from event averaging. In fact the algorithm Eq. (16) for Standard Wigner followed from assuming precise values simultaneously for both space and momentum. This is clearly evidenced [7] in the factor 8 in Eq. (16) in what is supposed to be the formula for a probability. One cannot simultaneously define both position and momentum for a cascading particle. If probabilities for coalescence are not in general large for small spatial separation, and if one averages sufficiently in each ion-ion collision, then this distinction may not be numerically too significant. Nevertheless, it is surely safer to employ Eqs. (6,7) rather than Eq. (16). Also at least part of the important physics lies in assigning wave packet sizes. Figs. 5,6 comparing ARC to the two Wigner calculations demonstrate that some price in absolute normalisation of the deuteron yields must be paid. The relative normalisation of Standard Wigner to ARC Dynamic changes appreciably between central and peripheral collisions. Clearly, Static coalescence, and its equivalent partner Quantum Wigner, contain a size parameter. The dynamic modeling permits this parameter to be internally estimated, yielding a higher degree of predictability.

We might offer as metaphor for microscopic rendering of coalescence an analogy with either deuteron stripping in finite nuclei and/or inelastic scattering. The latter gives one a more directly comparable expression for the probability displayed in Eq. (6), but the former, stripping analogy, could give a more concrete model if pursued. Both formalisms applied to the system of neutron+comoving nucleons, after the short range interactions between cascading particles have ceased, suggest using neutron and proton wave packets defined in the long range field generated by the comovers. Although it is far from trivial to evaluate this field, our dynamic approach may be viewed as making a first estimate of its spatial extent. The numerical results are encouraging. It would seem perhaps only the spatial extent of the particle wave functions play a role, the details of the field not being overly significant. We reiterate that this field is weak, long ranged and would little affect the single nucleon distributions.

III. DYNAMIC COALESCENCE: IMPLEMENTATION INTO ARC.

Since the functions f_p, f_n in Eq. (8) describe the distribution of centers and average momenta of nucleon wave packets as generated by the cascade, we were led to write for the minimal quantal treatments, i.e. for ARC Dynamic, Static or for the quantal Wigner

$$n_d = \frac{3}{4} \sum_{ij} C(\mathbf{x}_{n_i}, \mathbf{k}_{n_i}; \mathbf{x}_{p_j}, \mathbf{k}_{p_j}), \quad (18)$$

where the sum in Eq. (9) can be restricted to np pairs with fixed kinematics, e.g. given rapidity and transverse mass. Indeed, as we have shown above, Quantum Wigner is just ARC Static with a fixed, likely small, size parameter, $r_{wp} = 1fm$ or equivalently $\sigma = 0.817fm$.

Specifically, our procedure within the simulation is to select pairs of nucleons, one neutron and one proton, follow their trajectories until both have ceased interacting with other hadrons and then evaluate, within a Monte-Carlo

framework, the possibility of coalescence. Should this occur, the nucleons are removed from the particle lists and replaced by the appropriate deuteron. Although in some low probability coalescence events one may find appreciable non-conservation of energy, conservation of momentum is guaranteed. The effect of this on the results is necessarily small and the non-conservation of energy limited to a few hundred MeV in a Au+Au collision. This is repeated for all choices of the pair within one ion-ion collision. As stated previously, it is assumed that deuterons formed before the cessation of interactions will not survive. Not only does the simulation, event by event, generate the nucleon precursor average positions and momenta, it also can guide us towards an evaluation of the size of their wave packets. The interaction history of the nucleons before freezeout can be used to estimate a radius for the fireball, and hence yield a value for the parameters σ_i , or since we have taken the neutron and proton size parameters equal and related these to the deuteron center of mass size, for a single σ . This σ will vary with the environment of the selected pair, impact parameter and perhaps also with the kinematics of the reaction. This better understanding of the relativistic and hence spatial aspects of cluster formation requires a more integrated version of coalescence within the cascade dynamics. In the next section we present model calculations and compare them to existing data.

From Eq. (7) it is clear that within the assumptions we have made, the relative position

$$\mathbf{x} = \mathbf{x}_n - \mathbf{x}_p \quad (19)$$

and momentum

$$\mathbf{k} = \frac{\mathbf{k}_n - \mathbf{k}_p}{2} \quad (20)$$

are the only classical variables entering the overlap calculation. A central question then is the choice of neutron and proton wave functions within the ion-ion simulation. The n,p wave packet product represents an initial two nucleon wave function, which we imagine prepared at a coalescence time contemporaneous with the last interaction of both nucleons, i.e. at $t_c = \max(t_n, t_p)$. The relative position and momentum are then evaluated in the two particle cm frame, and from these the chance of coalescence determined. In the Static case the probability is calculated in Eqs. (7,8) with a wave packet size fixed for all pairs. In Dynamic the wave packet size is estimated separately for each pair, using the distribution of previous interactants.

It is reasonably evident that only particles in the backward light-cone of the coalescing pair should define the nucleon and deuteron cm wave packet size. We draw the light cone at the coalescence point (see Fig. 19), $x_c^\mu = (x_c, t_c)$, whose spatial coordinates lie at the midpoint of the coalescing np pair in their mutual cm frame. Moreover, since coalescence occurs only after freezeout, one must make this determination as late as possible. The option which suggest itself as most consistent with these constraints is propagation of the co-interactants as closely as possible to the light-cone of the coalescing pair (again see Fig. 19). Alternatively, one could calculate an average position for the interacting particles in the backward light-cone, or use their initial positions. We will discuss the numerical effects of alternatives. Spectators are generally neglected in the calculation of wave packet sizes as are particles causally disconnected from the coalescence. However, for deuterons coalescing purely from spectators, the Dynamic calculation of size includes only spectators. The assumption made here is that the initial nucleus size determines the wave packet of these essentially undisturbed nucleons. The wave packet size is equated, in Dynamic, to the rms radius of the interacting particle region. All quantities necessary for calculation of coalescence are now available, and there remains only the decision by Monte Carlo whether or not coalescence actually takes place. There is no double counting, nucleons forming deuterons are removed from the particle lists.

Static coalescence, for which wave packet sizes are assigned externally, might simulate Dynamic if for example sizes were adjusted to account for expected changes in interaction region size, as for example seen in central and peripheral collisions. We will see that for the systems considered here i.e. for Si+Au, the different routes followed lead to quantitatively altered outcomes, at least in overall normalisation. The dynamic simulations seem, however, to give a consistently accurate picture of existing AGS experiments.

IV. RESULTS

Comparison is made between experiment and coalescence theory for various choices, Static, Dynamic or Wigner. One might expect the Standard Wigner to be essentially equivalent to the static theory for a small wave packet radius assignment, perhaps ~ 1 fermi. This, as we shall see, is not so. An overall picture of the differences that arise is exhibited in Figs. 5,6 for Si+Au.

The ARC Dynamic $\frac{dN}{dy}$ spectra in Fig. 4 constitute a comprehensive normalisation of deuteron production. Perhaps because the cascade seems to work so well for absolute deuteron yields as well as for the detailed transverse-mass and rapidity spectra, one can eventually extract information about the interaction region. Later, in Figs. 13 to 17, we tie

the parentage of the deuterons to their emerging rapidity. For existing E802 data on Si+Au the less disrupted target nucleons play a large role, especially at small laboratory rapidity. This will not be the case for a central Au+Au collision where dominantly, fully interacting neutrons and protons coalesce. We await more comprehensive data for the gold projectiles to illuminate what might be the most interesting aspects of this study.

We begin with deuteron production for the reaction Si+Au at 14.6 GeV/c. Figures 1 and 2 contain a principal result of this paper, a comparison between ARC Dynamic and AGS E802 data [24], for transverse-mass proton and deuteron spectra obtained both peripherally and centrally. Figures 3 and 4, containing rapidity spectra, are essentially obtained from Figs. 1 and 2 by integration, although in the case of the experimental spectra some care must be taken to define this integration. The experimental triggers defining centrality and peripherality [24] are imposed in the theoretical analysis. There is less dependence on these triggers for central than for peripheral simulation. In the latter case E802 has used a different, lower, ZCAL [24] cut for the most forward angle slice. We have employed a single average cut and attempted to compensate for the forward trigger in that fashion.

The wave packet size parameters used for Dynamic are determined within the simulation, separately for each pair. The deuteron internal, or relative, wave function is defined by:

$$\alpha = 1.76 fm \tag{21}$$

fixed to yield the correct electron scattering radius [20,21]

$$r_d = (3/2)^{1/2} 1.76 fm = 2.15 fm. \tag{22}$$

If one corrects for a finite proton charge radius, $r_p \sim 0.8 fm.$, the appropriate point nucleon distribution is described by $r_d = 1.91 fm$ and $\alpha = 1.56 fm$. We compare yields with both choices of deuteron radius, to test for sensitivity to the internal deuteron wave function.

Clearly, on a global level, dynamic coalescence does very well indeed. It is difficult to isolate any systemic discrepancy between measurement and simulation although differences, generally $\sim 10\%$, are on rare occasions as large as 30-50%. Just to what degree these very reasonable theoretical descriptions of the experimental data, are subject to assumptions and choice of "parameters" we explore below. We emphasize that the calculated deuteron and proton spectra are absolutely normalized by the cascade dynamics with no free parameters; by "parameter" we here mean quantities like r_d . These results then suggest the present approach to coalescence may add a useful tool in the search for interesting medium dependences. Given the quadratic dependence of deuterons on individual nucleon distributions, one must of course do reasonably well quantitatively, in order to ascribe apparent deviations from experiment to interesting medium dependence. Surprisingly, theory-experiment differences are smaller for central collisions for which better quality data exists but in which physics not described in the cascade is more likely present.

No matter how one extracts inverse slopes, or "temperatures", from the experimental or theoretical data, Fig. 1 and Fig. 2 attest to only small differences between measurement and calculation. For Si+Au, ARC in the dynamic mode closely reproduces the dependence on transverse mass seen experimentally, in both shape and magnitude. Figs. 3 and 4 highlight the accord between theoretical and measured overall magnitudes.

The E802 rapidity distributions are obtained by fitting a single exponential to the m_t spectra and after extrapolation into unmeasured regions. The theoretical $\frac{dN}{dy}$'s are directly integrated without any such fitting or extrapolation. To the extent that the transverse spectra are single exponentials, only small additional differences are introduced in the rapidity spectra. Nevertheless, much larger apparent differences may be present for the "temperatures" extracted from the experimental data. In a few instances, for the highest rapidities cited by the E802 collaboration, the deuteron data quality does not support a reliable slope determination. It is probably better to just compare simulation and measurement directly and in the case of good agreement to use the theory to extract a "temperature". In any case the simulations present temperatures close to experiment in both magnitude and in kinematic dependences. The deuteron slopes depart somewhat from the limit of gaussian convolution of neutron + proton m_t distributions, giving on occasion higher than naively expected temperatures, but this feature is well mapped in the cascade.

One should note again that our comparison with experiment begins at a laboratory rapidity of 0.5 and stops well short of the projectile rapidity. In extreme peripheral collisions where the nuclei are only mildly excited and nucleons and clusters simply boil off there is some question about pure coalescence. Just at $y_{lab} < 0.5$, Figs. 3 and 4 show a slight hint of calculation falling below measurements. However, examination of Fig. 15, which makes explicit the parentage of coalesced particles, indicates that by $y_{lab} = 0.5$ calculated deuterons are already dominated by s-i pairs and not by purely s-s. This hint may then be illusory (see also the caption for Fig. 3). In any case measurements at lower rapidity would not be amiss.

Comparison of Wigner type calculations with ARC is seen in Figures 5,6. There are, as we noted, two approaches to the Wigner formalism. Some quantal aspects can be retained in evaluating the coalescence overlap, whence Wigner is identical to ARC Static. In such a case it would seem reasonable to assume the smearing in the neutron and proton

wave packets is small, perhaps near to 1 fermi. This we have labeled “Quantum” Wigner in Figs. 5 and 6. The result is a significant reduction, by close to 50%, in deuteron yield. The second approach is the Standard Wigner which inserts sharp definitions of both nucleon position and momenta in the calculation of deuteron content. The result of this ad hoc assumption, at best an approximation to the quantum dynamics, cannot be compensated for by the later averaging over nucleon distributions inherent in a single cascade collision, nor by event averaging. What is evident from these figures is the changing ratio of Standard Wigner to ARC Dynamic as one proceeds from central to peripheral and in the latter case especially as one moves towards mid rapidity. As we indicate in the next section on space-time structure, there are several components in the coalescing deuterons, spectator-spectator, interacting-spectator and interacting-interacting. Because of our rapidity cuts $y_{lab} > 0.5$ the s-s plays little role here, but the coalescence of target based nucleons is still important for the Si+Au system [15], at least for measurements at less than mid-rapidity.

In Figs. 7,8,9 and 10 the evolution of Static coalescence with a globally specified wave packet size is explored. There is no way to assign a unique radius to the packets, but considering the close relation to the oft used Wigner paradigm, it is very interesting to pursue this evolution. Clearly for both central and peripheral analyses there is an “optimum” size. This is already apparent in the rapidity distributions displayed parametrically in Figs. 7 and 8, but more evident in Figs. 9 and 10 where the magnitudes for selected rapidities are plotted against σ , the parameter entering the gaussian wave functions. The position of maximum yield, σ_{max} , changes with impact parameter $\sigma_{max} \sim 2fm$ for a central collision and somewhat smaller, $\sigma_{max} \sim 1.25fm$, for peripheral. These correspond to wave packet radii of $2.5fm$ and $1.5fm$ respectively. This variation with size is not insignificant since much of the physics is contained in the absolute magnitudes. Static calculations made near these sizes, producing the magnitudes comparable to Dynamic, also exhibit transverse mass distributions close to those in Dynamic. Standard Wigner central m_t spectra are again essentially indistinguishable from ARC. However, peripheral Standard Wigner, for which one might have expected the basic assumptions to be more valid, produces somewhat higher slopes, i.e. lower temperatures than seen in ARC or in experiment.

Finally, in contrasting Static and Dynamic we note that use of a static size parameter choice somewhat below σ_{max} (see Fig. 14) yields agreement between these calculations for the central, but a bit above this value for peripheral.

We have not presented comparative plots, within Dynamic, for alternative definitions of the “past history” of a coalescing pair, though this choice in principle determines the important wave size. This is because the results are essentially identical, at least within the accuracy justified by present experiments, for a wide variety of alternatives.

Explicit comparison of the effect on deuteron yield of changing the deuteron internal radius from the point to the charge value is presented in Figs. 11,12. Similar small variation is found with the standard Wigner form factor, indicating that use of more sophisticated wave deuteron wave functions [13] is unlikely to significantly change results within that approach. Also tested was the sensitivity of theory to the actual experimental triggers: peripheral spectra are sensitive to changes in these “cuts”, central considerably less so.

Finally, we have examined the dependence of our results on the energy cutoff used to halt the cascade. All present calculations were done using a kinetic energy lower limit $T_{cut}(cm) = 30 MeV$ for elastic collisions. We reran some cases, both Wigner and Dynamic, for $T_{cut}(cm) = 15 MeV$, finding less than 10% reductions for the lowest rapidities in central collisions and less at higher rapidities, while for peripheral collisions slight increases. Within the accuracy of the present theory these are negligible changes. To do better would require a much more detailed dynamics, including deuteron breakup and reformation between the times corresponding to the energy cutoffs..

The distributions of precursor nucleon wave packet sizes extracted in the dynamic treatment are displayed and discussed in the next section. The figures in that section also exhibit the parentage of the coalescing pair, divided into three self-descriptive classes, spectator-spectator, spectator-interacting and interacting-interacting.

V. SPACE, TIME AND MOMENTUM STRUCTURE OF COALESCING PAIRS

It is of great interest to display the space-time history of pairs near the freezeout time t_c , for nucleons which both succeed and fail to coalesce. Figs. 13-17 contain such information for the Dynamic simulations. Fig. 14 succinctly summarizes the information most immediately relevant to the comparison with E802 data pursued extensively in this paper. The deuteron data [24] extends over the rapidity range $0.5 \leq y_{lab} \leq 1.5$ for centrally defined collisions, and a somewhat more abbreviated range for peripheral. Consequently, in the upper two graphs of Fig. 14 we impose a cut $y_{lab} > 0.5$ and display the scatter plot of wave packet size r_{wp} vs rapidity for coalesced np pairs embedded in a background of all pairs, for both central and peripheral. The lower two graphs in this figure are simple histograms for these two sets vs r_{wp} . One concludes from the lower graphs that the average r_{wp} for all pairs is considerably larger than for the coalesced pairs; for either central or peripheral the overall averages are close to $5fm$, while the coalesced averages are:

$$\langle r_{wp}(central) \rangle = 2.59 fm \quad (23)$$

and

$$\langle r_{wp}(peripheral) \rangle = 1.67 fm \quad (24)$$

respectively. These values are in good accord with the variation of deuteron yields vs wave packet size for Static, (see Figs. 9,10) insofar as such global choices for r_{wp} would result in Static $\frac{dN}{dy}$'s close to those from Dynamic. Fig. 13, containing similar plots but with no rapidity cut, tells a different story. The deuterons which fall near $y_{lab} = 0$ arise from target particles experiencing only gentle interactions and consequently from larger r_{wp} . This is especially clear in the peripheral histograms in this figure, where two distinct groups of pairs are seen, one at the target "size" and another for more strongly interacting progenitors at a reduced size.

The average $r_{wp} = 1.67 fm$ for peripheral collisions of Si with Au is perhaps not much larger than one might have assigned *ab initio* in the Quantum Wigner [25]. But the rather steep dependence of yields on the size parameter in Figs. 9,10 is fair warning that such a choice is better made dynamically. The central $r_{wp} = 2.59 fm$ is appreciably larger but still implies a rather restricted spread in the neutron and proton wave packets. The dynamic picture is remarkably consistent.

Further interesting information may be gleaned from Fig. 15 on time evolution of coalescence and from Figs. 16,17 concerning the relative separations of the coalescing pairs in position and momentum, ΔX_{np} and ΔP_{np} . In particular the range of permissible relative momenta is severely restrictive, relative momenta larger than 100 MeV/c are rarely seen for a coalesced pair; a sign of course that the deuteron is a quite low energy object, weakly held together.

In most figures in this section we have tried to indicate the parentage of the coalescing pairs, consisting of three groups corresponding roughly to spectator-spectator, spectator-interacting and interacting-interacting. There is a further division into target and projectile very closely identified by rapidity, i.e. from target to mid-rapidity most deuterons consist of two target particles while beyond mid-rapidity projectile particles dominate. There are a few deuterons formed from one target and one projectile particle at mid-rapidities, but not many.

VI. SUMMARY AND CONCLUSIONS

A rather comprehensive investigation of the coalescence model of deuteron production in a cascade environment has been carried out for a heavy-ion pair for which extensive data exists, i.e. Si+Au. The principal physical assumption made is that deuterons survive to maturity only if their component nucleons have ceased interacting before coalescence. This assumption allows one to factor the theoretical calculation into a piece depending on the cascade and a piece depending on the dynamics of coalescence. If, after factorisation, one is to include quantum mechanics within the formation dynamics then some knowledge of the spatial and momentum spreading in the nucleon pair wave functions is required. Dynamic coalescence provides this knowledge and seems to give a good broad-based description of the measurements. Use of this mechanism to predict Au+Au deuteron yields, at present AGS energies as in Fig. 18, and for lower energies where this massive system is more likely to be dominantly equilibrated, then seems justified. The static paradigm provides a reasonable, and computationally swifter, description of the data once the global choice for the wave packet parametrisation is made, but as we have said much of the interesting physics may lie in this choice. Further, the size parameter r_{wp} is a function of the collision environment, significantly larger for a central collisions, and certainly varying with rapidity.

Alternative approaches, both Static and Standard Wigner, either requiring or not the specification of a size parameter, can also apparently give an acceptable description of the m_t "angular" distributions but do not provide a completely unified picture of their normalisation. In particular the evolution of $\frac{dN}{dy}$ from target to mid-rapidities, and again from peripheral to central is not always correctly tracked. Moreover, the most interesting deviations from the cascade dynamics, occasioned by high densities achieved for lengthy times during collision, may well be expected to appear in overall normalisation. For example plasma formation might increase the time till freezeout and consequently the freezeout volume, thus suppressing deuteron formation. Excitation functions of deuteron production and other interesting observables, will be available in the near future at AGS energies of 2-8 GeV/c, i.e. just where high densities in a truly equilibrated system might more reasonably be expected [19]. One will then have deuteron data below and above the interesting region and a drop in yield relative to that expected from the pure hadronic simulation would be very interesting indeed. ARC should provide a good predictive background against which to measure these functions in a search for unexpected and interesting deviation, i.e. genuine medium effects. We will in future work present a theoretical analysis of the Au+Au excitation functions in this energy range.

Anti-deuteron formation can be described by the same picture. A simple rule, which ought to work well for rapidity distributions, would be to extract the ratio

$$\rho = \frac{\left[\frac{dN}{dy}\right]_d}{\left[\frac{dN}{dy}\right]_p \left[\frac{dN}{dy}\right]_n} \quad (25)$$

from the present calculations and then to construct

$$\left[\frac{dN}{dy}\right]_{\bar{d}} = \rho \left[\frac{dN}{dy}\right]_{\bar{p}} \left[\frac{dN}{dy}\right]_{\bar{n}} . \quad (26)$$

This evaluation would probably provide adequate numerical accuracy and would save the considerable computing time required to give passable statistics. The distributions of anti-protons and anti-neutrons, predicted by the cascade [26] in Eq. (26) would of course significantly modify the predictions for \bar{d} 's in both shape and magnitude. It is unlikely, however, that more information will obtain from such measurements on the Si+Au system, as exotic as they might be. For Au+Au the increased baryon densities expected and the tendency of anti-particles to annihilate might produce an interesting interplay. ARC calculation of anti-particle production [26,27] finds that classical screening of annihilation at low energies diminishes the density effects, leading to anti-particle rapidity spectra somewhat narrowed at mid-rapidity, but not drastically different in shape than other massive produced particles. Again, new physics might arise from careful measurement of absolute yields. Both prediction and measurement of anti-deuteron crosssections are complicated by the limits in knowledge of \bar{p} production in pp collisions at AGS energies and by the paucity of anti-deuterons likely to be seen in the data.

In an earlier work [11] we considered more massive clusters and found it necessary to assign phase-space windows peculiar to each bound system. There is no barrier to extending the cluster baryon number in Dynamic, aside from the limitations of computing time. Simulation used for the design of heavy-ion detectors, for example a possible forward detector at RHIC, might need to study such massive clusters. We intend to pursue this extension within a time-saving algorithm.

This manuscript has been authored under DOE supported research Contract Nos. DE-FG02-93ER40768, DE-AC02-76CH00016, and DE-FG02-92 ER40699. One of us (Y. P.) would also like to acknowledge support from the Alfred P. Sloan Foundation.

References

- [1] S. T. Butler and C. A. Pearson, *Phys. Rev.* **129**, 836 (1963).
- [2] A. Schwarzschild and Č. Zupančič, *Phys. Rev.* **129**, 854 (1963).
- [3] E. A. Remler, *Ann. Phys. (NY)* **95**, 455 (1975)
E. A. Remler, *Phys. Lett.* **159B**, 81 (1985)
J. Aichelin, E. A. Remler, *Phys. Rev. C* **35**, 1291 (1987).
- [4] R. Bond, P. J. Johansen, S. E. Koonin and S. Garpman, *Phys. Lett.* **71B**, 43 (1977).
- [5] A. Z. Mekjan, *Phys. Rev.* **C17**, 1051, (1978).
- [6] J. I. Kapusta, *Phys. Rev.* **C21**,1301 (1980).
- [7] M. Gyulassy, K. Frankel, and E. A. Remler, *Nucl. Phys.* **A402**, 596 (1983).
- [8] S. Mrówczyński, *J. Phys. G* **13**, 1089 (1987).
- [9] P. Danielewicz, G. F. Bertsch, *Nucl. Phys.* **A533**, 712 (1991).
- [10] C. B. Dover, U. Heinz, E. Schnedermann, and J. Zimányi, *Phys. Rev. C* **44**, 1636 (1991).
- [11] A. Baltz, C. B. Dover, S. Kahana, Y. Pang, T. Schlagel, and E. Schnedermann, *Phys. Lett.* **325B**, 7 (1994).
- [12] R. Hanbury-Brown and R. Q. Twiss, *Nature*(London), **178** 1046(1956); G. Goldhaber, S. Golhaber, W. Lee, and A. Pais, *Phys. Rev.* **120**, 300 (1960); M. Gyulassy, S. K. Kaufmann and L. W. Wilson, *Phys. Rev.* **C20**, 2267 (1979); S. Pratt, *Phys. Rev. Lett.* **53**,1219 (1984); W. A. Zajc, in *Particle Production in Highly Excited Matter*, Nato ASI Ser. B, Physics Vol. 303.
- [13] J. L. Nagle, B. S. Kumar, M. J. Bennett, S. D. Coe, G. E. Diebold, J. K. Pope, H. Sorge, and J. P. Sullivan, *Phys. Rev. Lett.* **73**, 2417 (1994); J. L. Nagle et al, *Phys. Rev. Lett.* **73**, 1219 (1994).
- [14] S. E. Koonin, *Phys. Lett.* **70B**, 43 (1977).
- [15] Y. Pang, T. J. Schlagel, and S. H. Kahana, *Phys. Rev. Lett.* **68**, 2743, (1992).
- [16] T. J. Schlagel, S. H. Kahana, and Y. Pang, *Phys. Rev. Lett.* **69**, 3290, (1992).
- [17] E814 Collaboration, J. Barrette *et al*, *Phys. Rev. C* **45**, 819, (1992).
- [18] S. Mrówczyński, *Phys. Lett.* **B248**, 459 (1990).
- [19] S. H. Kahana, Y. Pang, and T. J. Schlagel, **HIPAGS '93**, MIT 13-15 Jan., 1993, Edited by G.S.F. Stephans, S.G. Steadman, and W.L. Kehoe.
- [20] S. Klarsfeld, J. Martorell, J. A. Oteo, M. Nishimura, and D. L. Sprung, *Nucl. Phys.* **A456**, 373 (1986).
- [21] C. W. de Jager, et al., *Atomic and Nuclear Data Tables* **14**, 479 (1974).
- [22] H. H. Gutbrod, A. Sandoval, P. J. Johansen, A. M. Poskanzer, J. Gosset, W. G. Meyer, G. D. Westfall, and R. Stock, *Phys. Rev. Lett.* **37**, 667 (1976).
- [23] M.- C. Lemaire, S. Nagamiya, S. Schnetzer, H. Steiner and I. Tanihata *Phys. Lett***85B**, 38 (1979).
- [24] T. Abbott et al, E802 Collaboration, *Phys. Rev.* **C50**,1024 (1994)
- [25] M. Gyulassy, private communication.
- [26] S. H. Kahana, Y. Pang, and T. J. Schlagel, *Phys. Rev.* **C47**, R1356, (1993).
- [27] E802 Collaboration, T. Abbott *et al* *Phys. Rev.* **C47**, R1351, (1993).

Central m_t Spectra : Si+Au @ 14.6 GeV/c

ARC Dynamic Coalescence vs E802

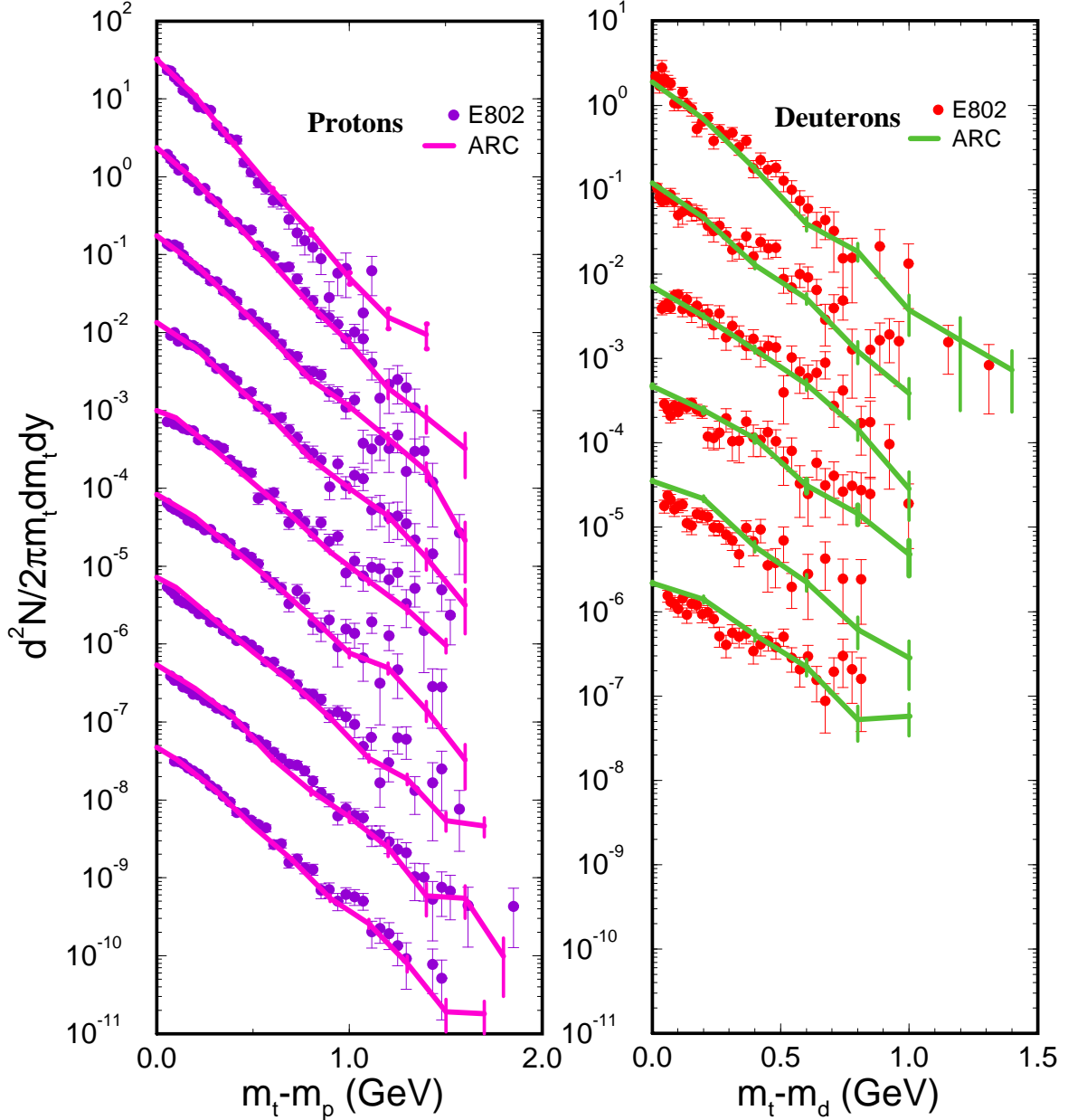


FIG. 1. Central Transverse Mass Spectra: ARC simulations are compared to E802 experiments. Dynamical coalescence determines the wave packet size for the coalescing nucleon pair, in this case after propagating their interacting comovers up to the pair light cone. There are then no free parameters in the theory, the deuteron relative wave function being characterised by the experimentally determined point size. There is little variation in these results with the deuteron size, at least, near the value $1.91fm$ used here. Using a different prescription for the propagation point, for example some “average” time in the past, also has very little effect. Centrality is fixed using the E802 specified TMA cut. Little sensitivity to this cut is evident here. We note the proton spectra in this figure and hereafter are automatically corrected for deuteron formation, i.e. coalescing protons (and neutrons) are removed from the cascade. Since the proton spectra enter essentially quadratically in deuteron formation, the theory is to be judged also by the matching to singles, a remark which applies to all further results.

Peripheral m_t Spectra : Si+Au @ 14.6 GeV/c

ARC Dynamic Coalescence vs E802

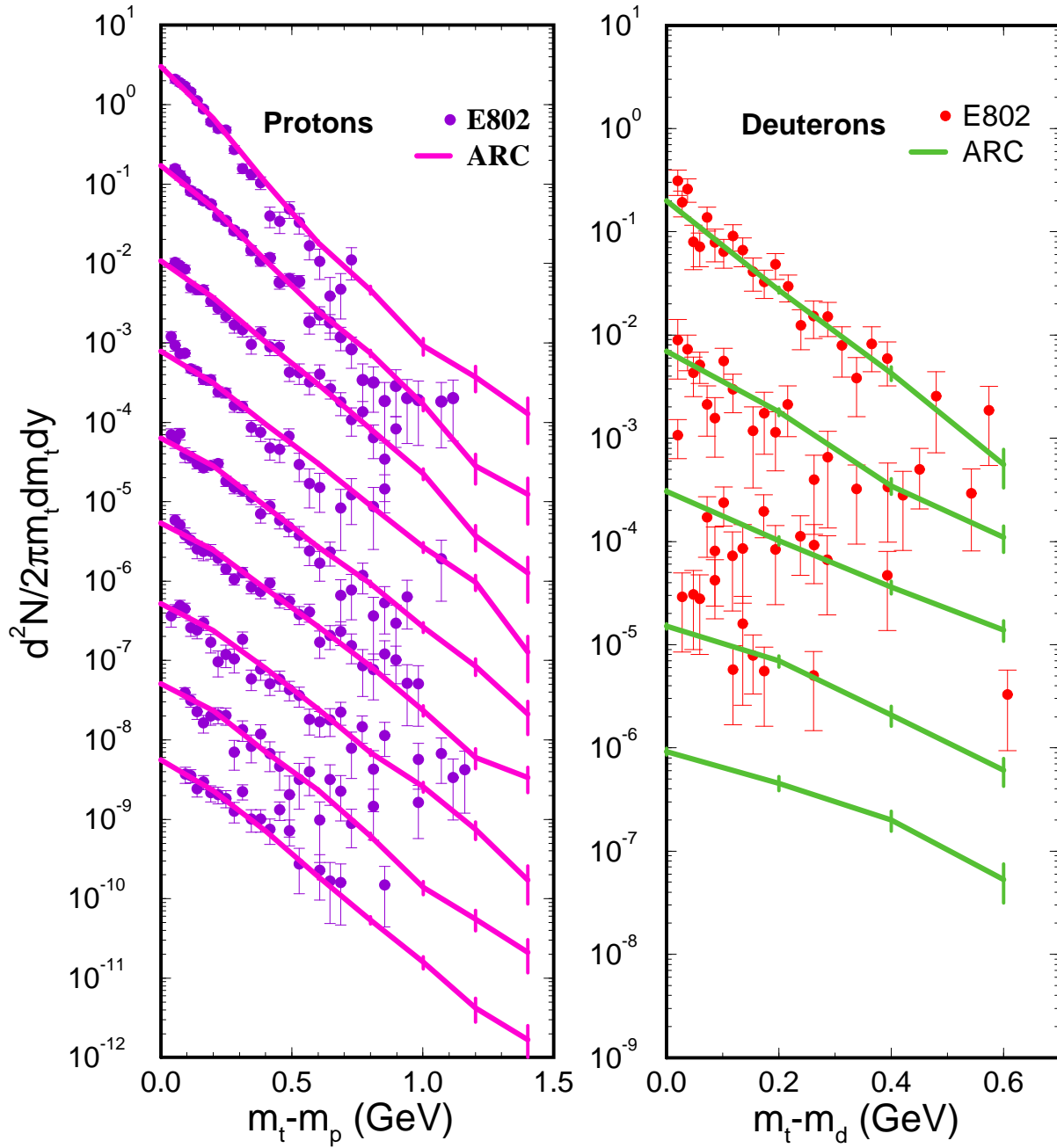


FIG. 2. Peripheral Transverse Mass spectra from ARC dynamical coalescence under the same circumstances as in Fig. 1. Peripherality is defined using an E802 prescription; there is greater sensitivity to this trigger than for central collisions. The proton spectra give some indication of the accord between the theoretical and experimental definitions of the trigger.

Central Deuterons :Si+Au 14.6 Gev/c

ARC Dynamic Coalescence vs E802

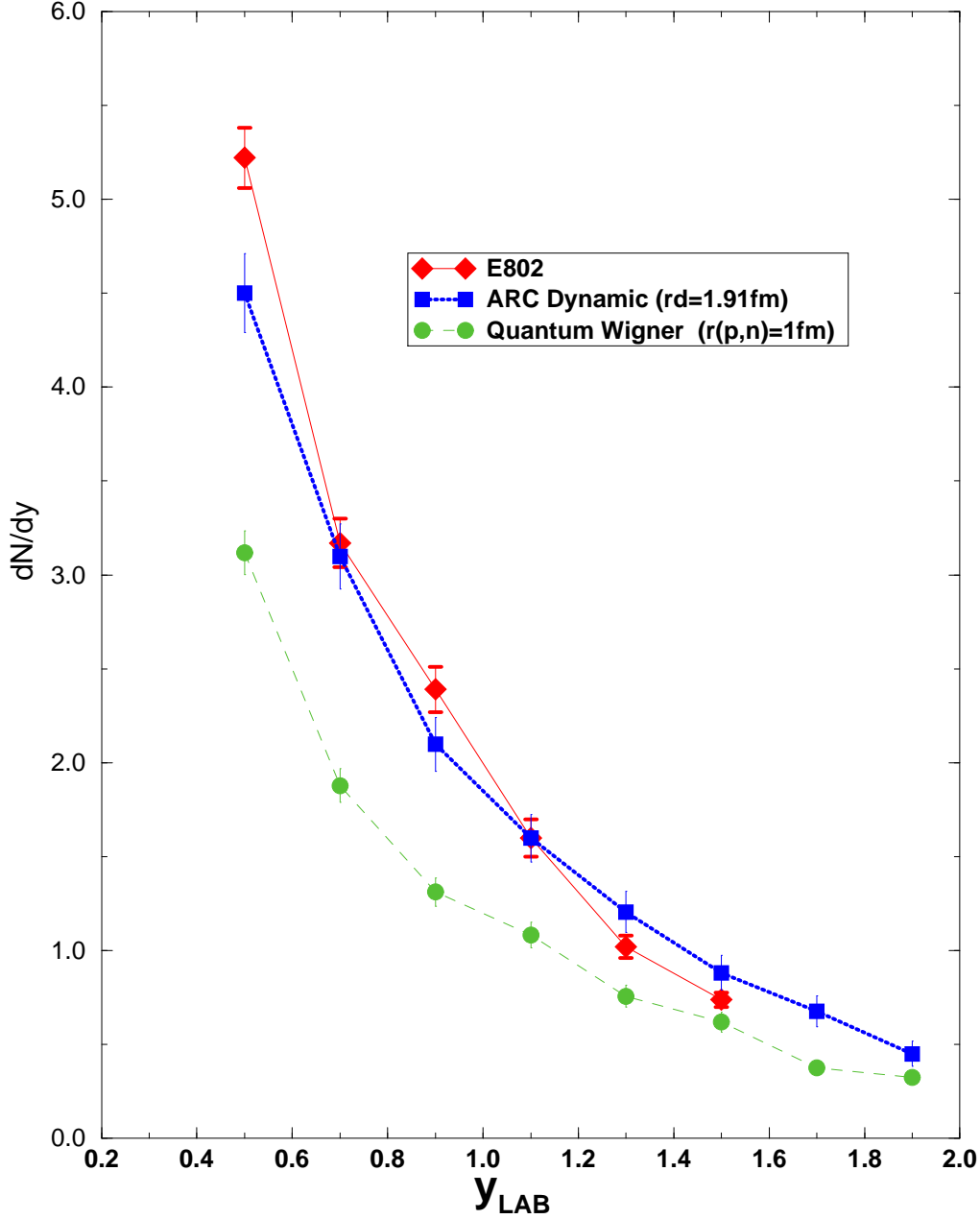


FIG. 3. Central Rapidity Distributions from dynamical coalescence are compared to experimental E802 values. The same, standard, light-cone prescription as described above and used for the m_t spectra in Figs. 1,2 has been applied. The theoretical $\frac{dN}{dY}$ is simply the integral over the m_t distribution; the E802 value is obtained after fitting to a single exponential and extrapolation. Differences in the comparison then arise for deviations from a simple exponential in Figs. 1,2. For example direct integration of the experimental m_t spectrum yields a lower value of $\frac{dN}{dY}$ than quoted by E802, resulting in central value for $y_{LAB} = 0.5$ of 4.83 rather than 5.23 and thus bringing theory closer to experiment. As indicated in the text the prescription Quantum Wigner in Fig. 3 is equivalent to ARC Static for a 1 fermi smearing of the neutron and proton wave packets, i.e. $\sigma = 0.817fm$.

Peripheral Deuterons : Si+Au 14.6 GeV/c

ARC Dynamic Coalescence vs E802

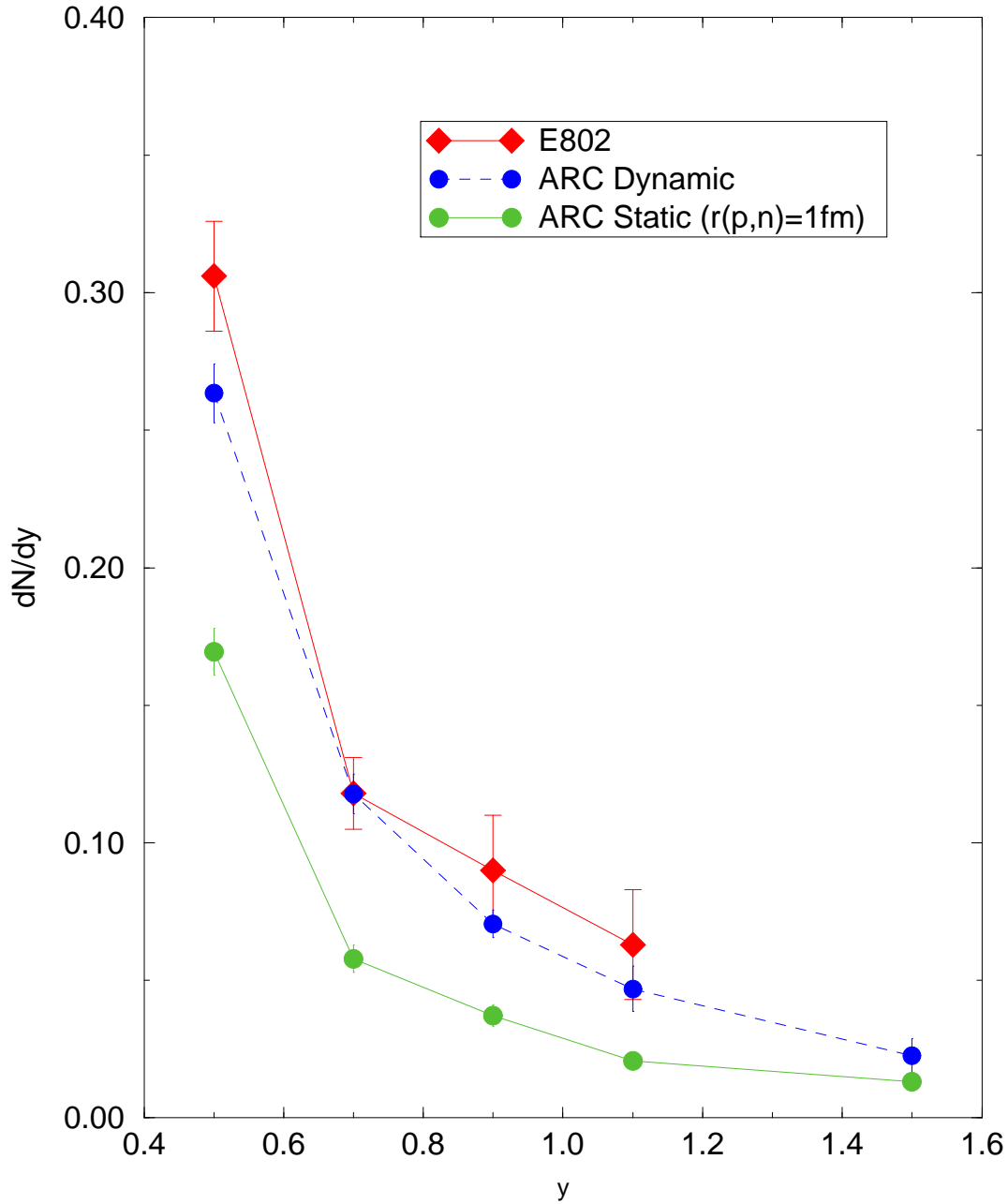


FIG. 4. Same as Fig. 3 but for peripheral Si+Au. We note again here the greater sensitivity to the application of the E802 defined peripherality using in this case ZCAL.

Deuteron Rapidity Distribution

Central Si+Au 14.6 GeV/c

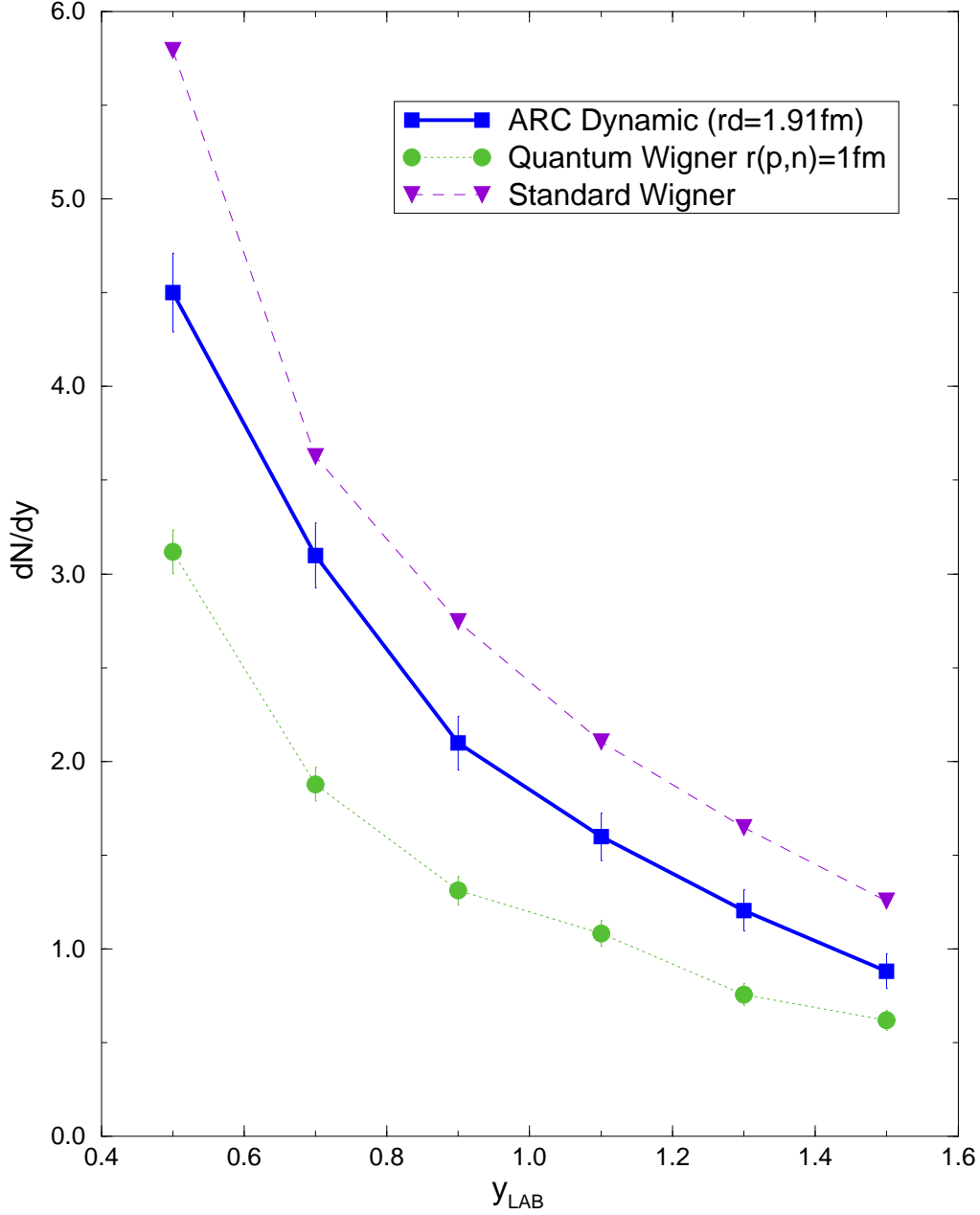


FIG. 5. Comparison between ARC Dynamic, Quantum Wigner and Standard Wigner (obtained using the form factor in Eq. (16)) for the Si+Au central rapidity deuterons. Quantum Wigner is identical to ARC Static for $\sigma \sim 1.25 fm$, i.e. $\langle r_{wp} \rangle \sim 1 fm$. Standard Wigner assumes the classical simulation can be characterised by point nucleons with sharp momenta. There is a factor of more than two between these two Wigner coalescence calculations. One notes also a similar comparison in Fig. 6 where Standard Wigner drops, at mid-rapidity, appreciably below the ARC Dynamic results.

Peripheral Deuterons : Si+Au 14.6 GeV/c

ARC Dynamic Coalescence vs E802

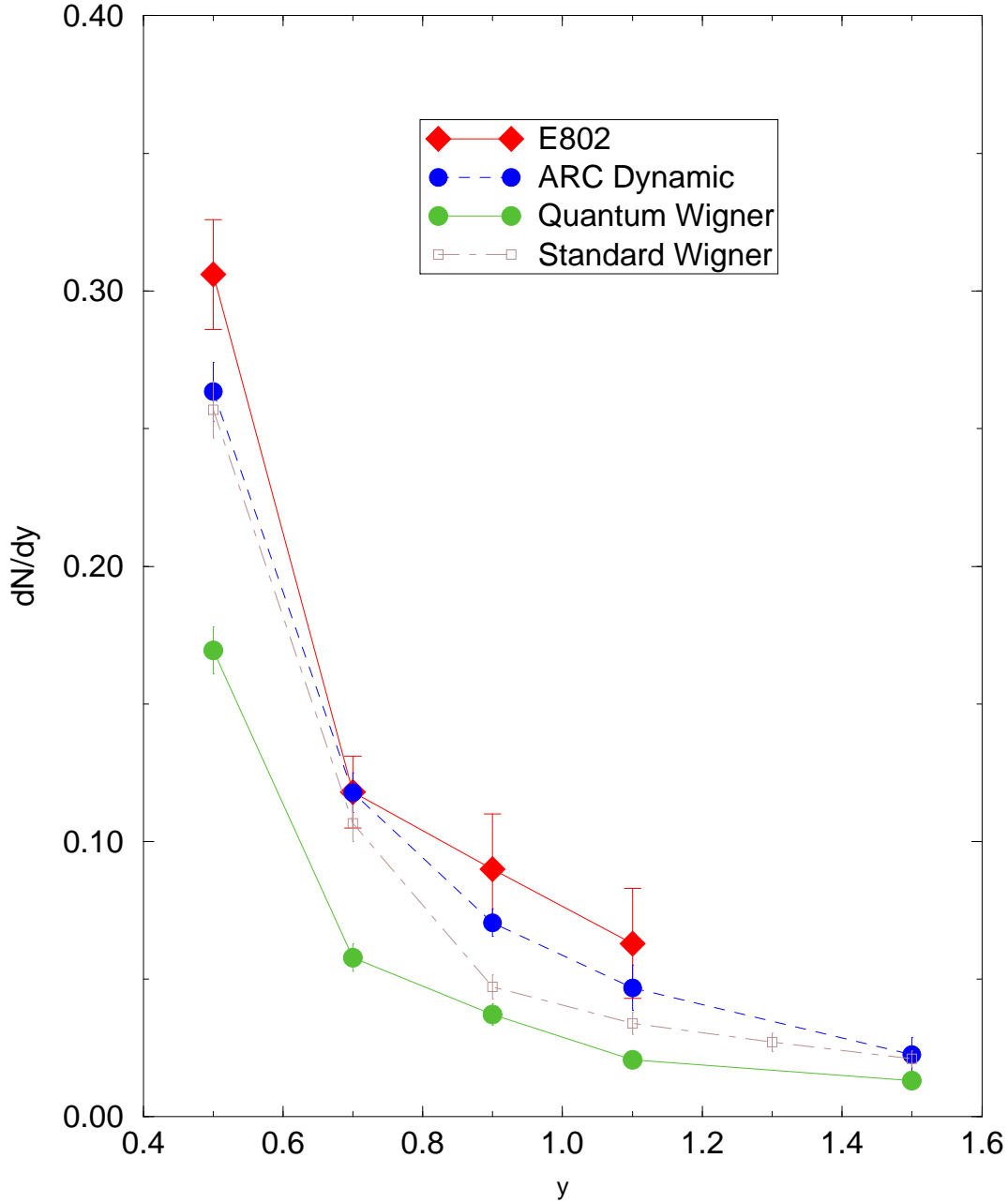


FIG. 6. Comparison between ARC Dynamic, Quantum Wigner and Standard Wigner (obtained using the form factor in Eq. (16)), but here for the Si+Au peripheral deuterons. The ratio of peripheral/central yields is close for ARC Dynamic and Quantum Wigner, but somewhat less for the Standard Wigner. The latter and ARC also present a changing profile as a function of rapidity, reflecting contrasting treatments of mainly target-target and target-projectile coalescences.

Static Coalescence Central Si+Au

Variation with Wave Packet Size

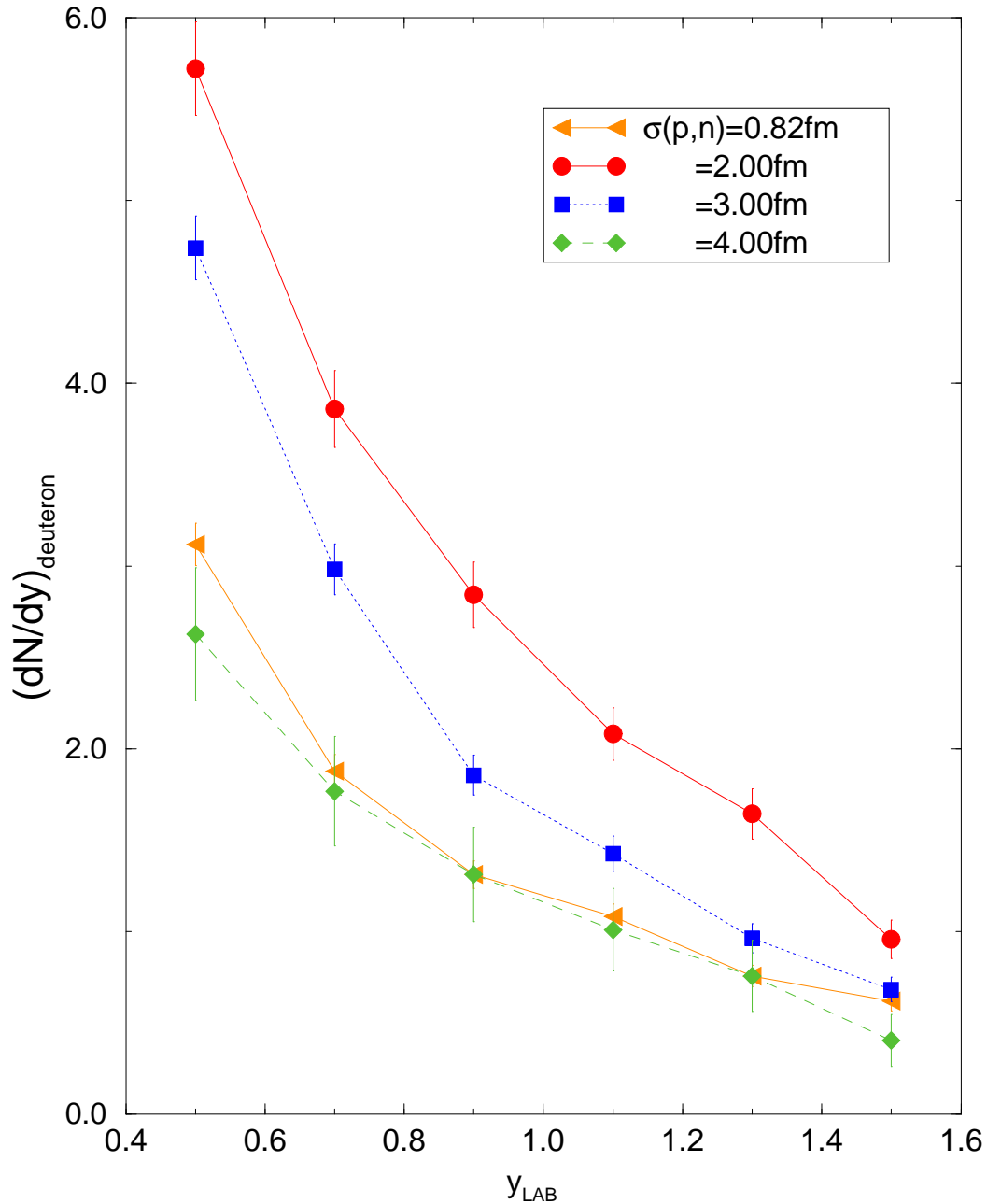


FIG. 7. The evolution with wave packet size of the ARC Static deuteron central rapidity spectra. There is a maximum in magnitude whose position in σ depends on the folding of the deuteron “content” in Eq. (6) with the ARC single neutron distributions in both position and momentum. The existence of the maximum is more explicit in Fig. 9 below.

Static Coalescence Peripheral Si+Au

Variation with Wave Packet Size

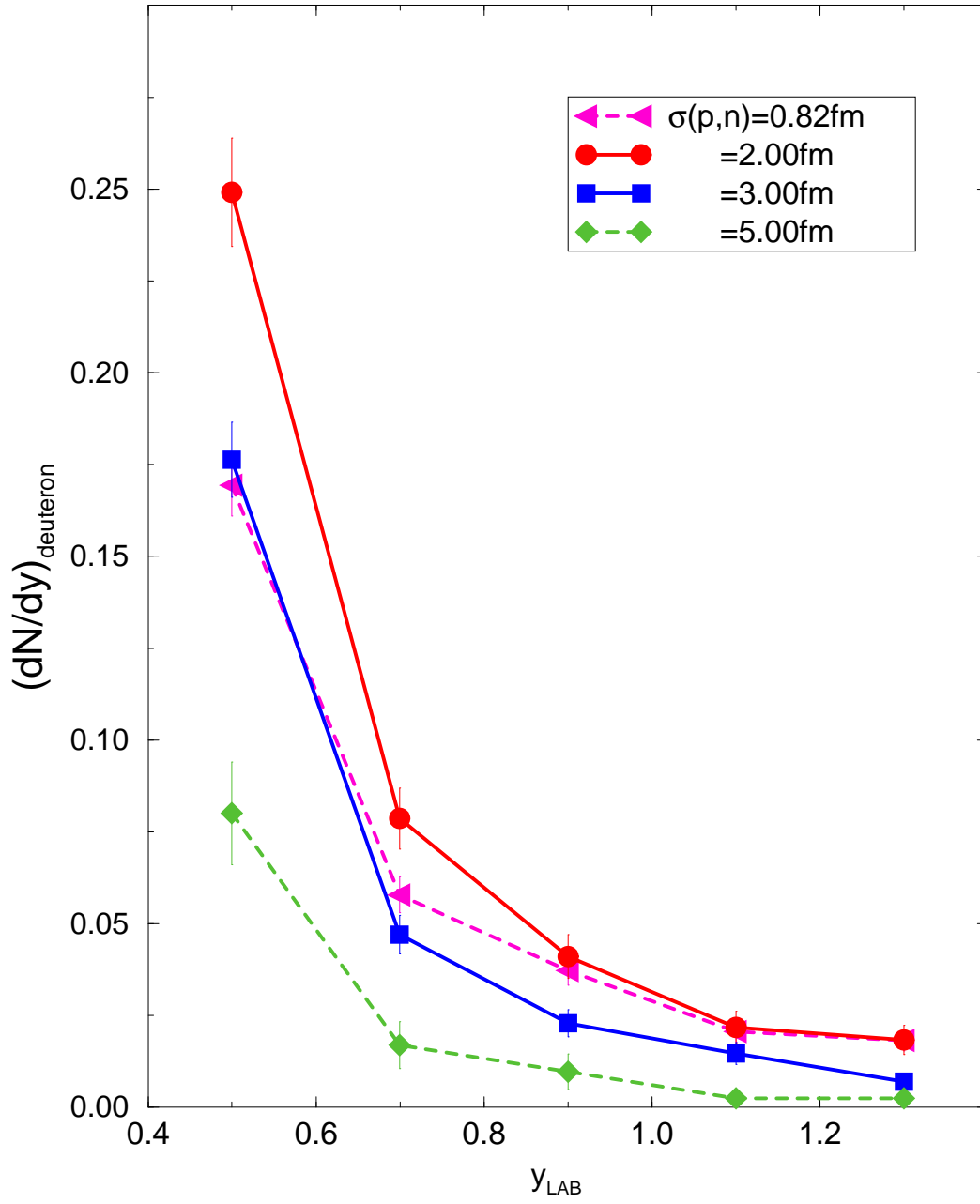


FIG. 8. The evolution with wave packet size of the ARC Static deuteron peripheral rapidity spectra. See also Fig. 10

Static Coalescence vs Size Parameter

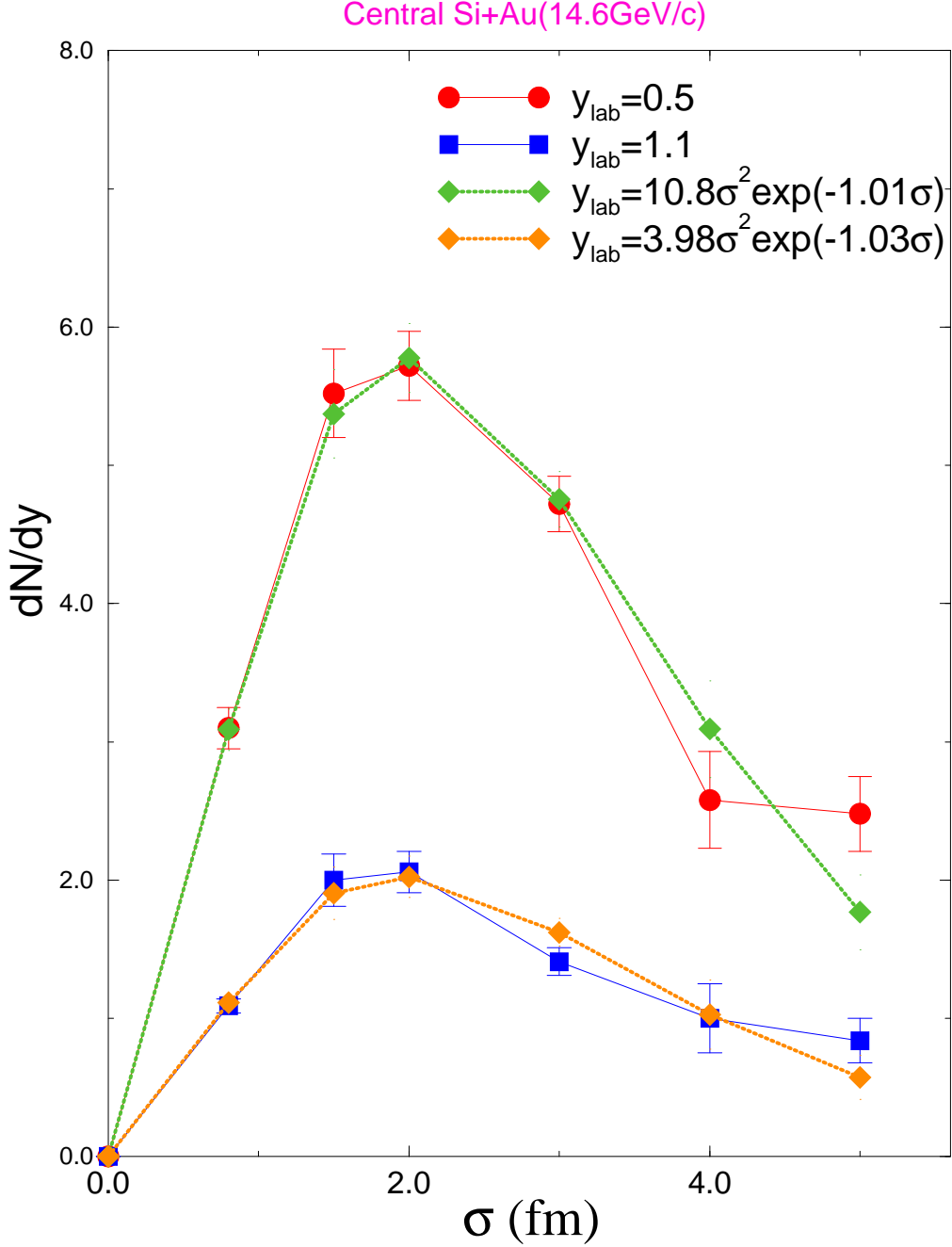


FIG. 9. Explicit variation of the central deuteron $\frac{dN}{dy}$ with size. Eq. (7) and the associated discussion suggest the overlap normalisation is maximized for $\sigma = \frac{\alpha}{\sqrt{2}}$, whereas clearly in this figure the maximum occurs nearer to $\sigma = 2.0$ for the differing Static simulations, demonstrating the importance of the wave packet dynamics. The variation is less marked for the higher, more forward, rapidity $y = 1.1$. Functions fitted to these ARC outputs are also indicated in this figure, and from these one can in fact extract the position of the maximum in $\frac{dN}{dy}$ to be close to $\sigma = 2$ for central.

Static Coalescence vs Size Parameter

Peripheral Si+Au(14.6GeV/c)

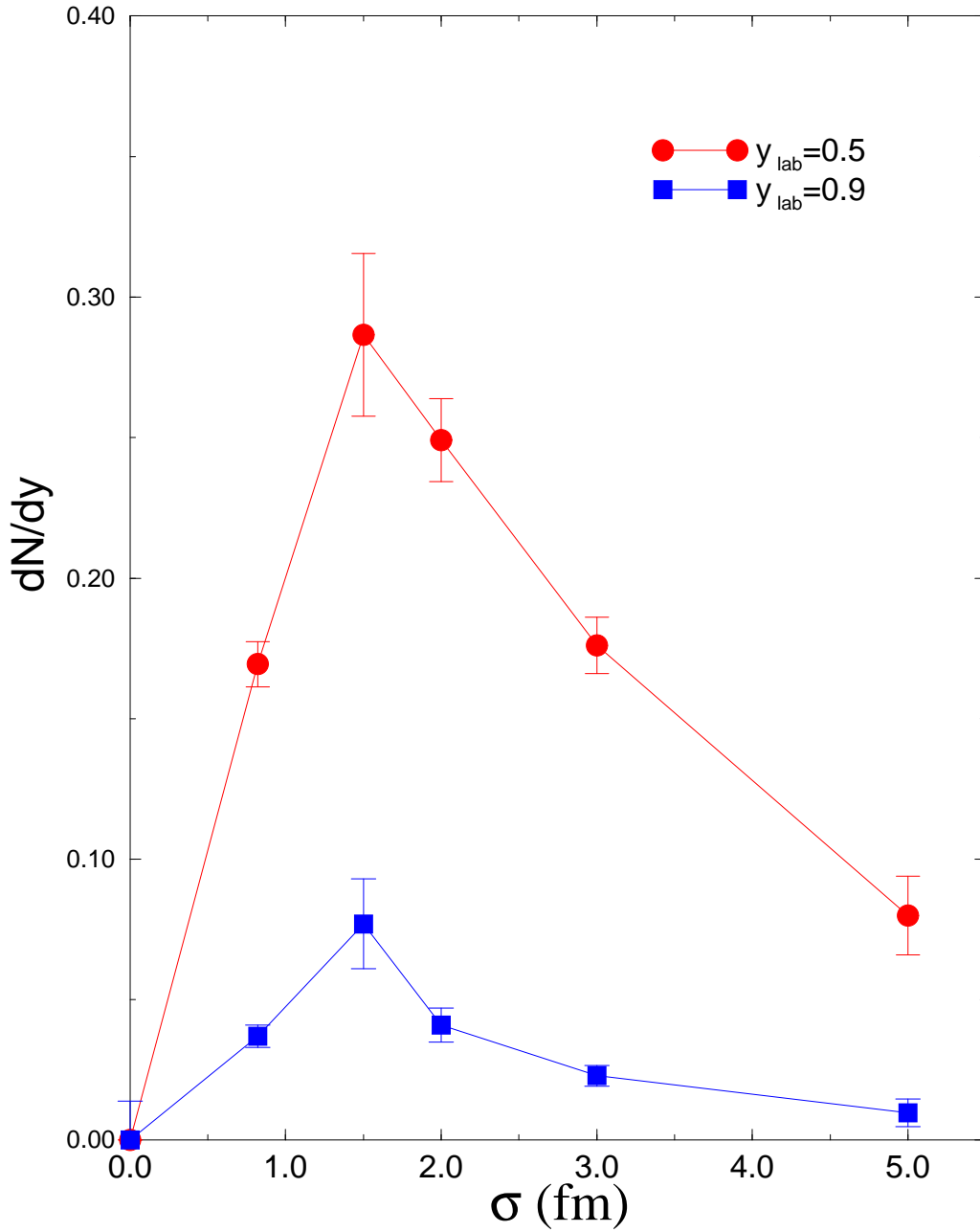


FIG. 10. Similar to Fig. 9, but for peripheral simulations. The maximum in $\frac{dN}{dy}$ is here below $\sigma = 2$.

Variation with Deuteron Radius

Peripheral Si+Au (14.6GeV/c)

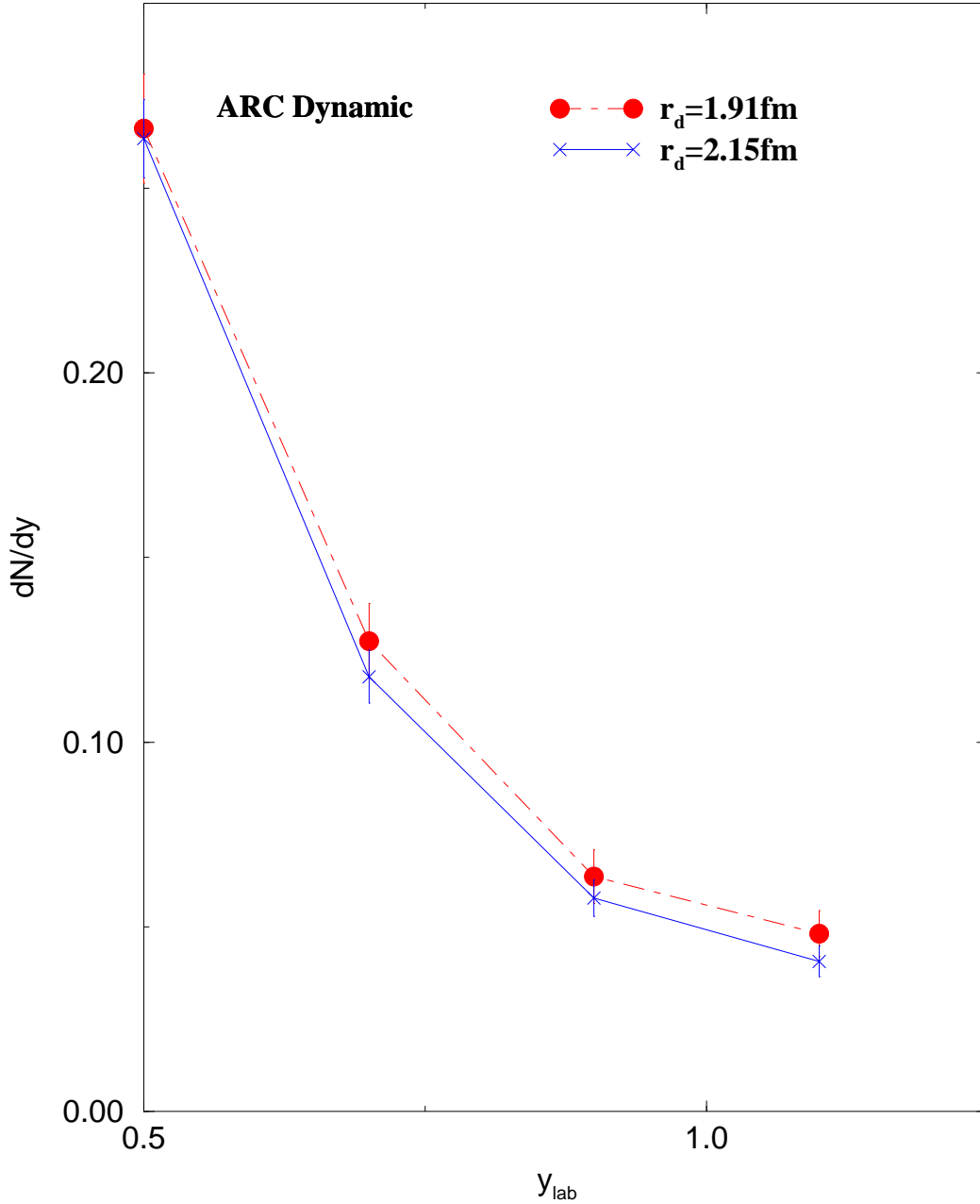


FIG. 11. Changes in peripheral rapidity spectra due to variation in the internal deuteron radius from its point nucleon value of $1.91 fm$ to the charge radius of $2.15 fm$ [21]. Both peripheral and central rapidity distributions show a weak dependence on this radius, at least near the actual physical values for the deuteron size.

Variation with Deuteron Radius

Central Si+Au (14.6GeV/c)

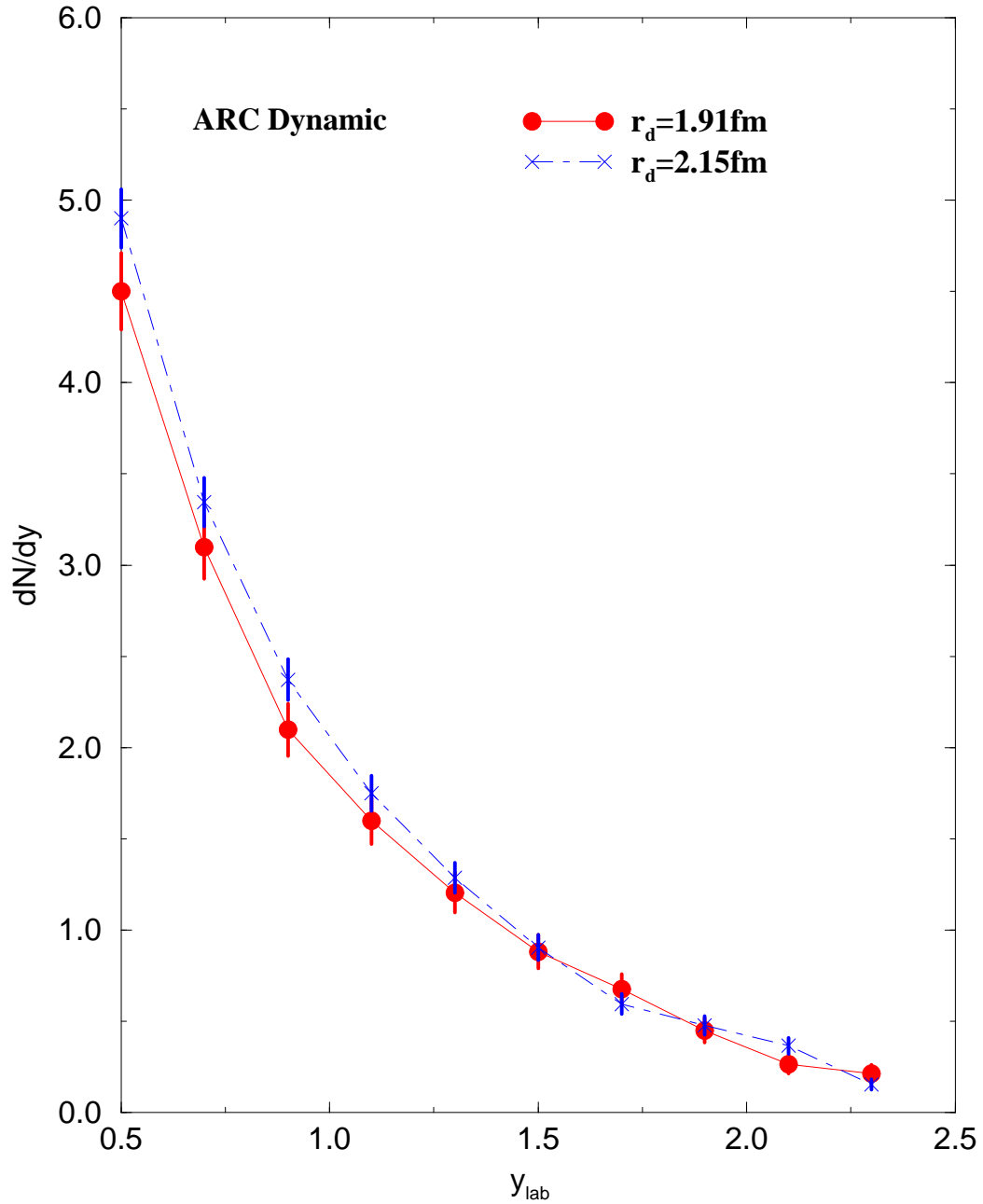


FIG. 12. Changes in central rapidity spectra due to the above variation in deuteron radius. Standard Wigner varies even less with this change in radius.

Included as fig13.jpg

FIG. 13. Progenitor Pair Sizes vs Rapidity, and Size Histograms: No rapidity cut. Wave packet spread in ARC Dynamic is displayed for all np pairs as well as for only coalesced pairs. In the upper two graphs scatter plots of all pairs are shown for both central and peripheral collisions: the three areas correspond to spectator-spectator (s-s, intermediate shading), spectator-interacting (s-i, light gray) and interacting-interacting (i-i, darkest shading). For peripheral collisions the separation into target and projectile is clear for the s-s pairs, with the larger sizes obtaining for the bigger gold nucleus; for central collisions there is no evidence of s-s pairs. In the lower two graphs the successful deuteron-forming pair-distributions are embedded in the overall histograms. Peripheral coalescence clearly contains (at least) two components, the smaller sizes correlated to i-i deuteron parentage, the larger, near $5fm$, to s-i and s-s.

Included as fig14.jpg

FIG. 14. Size vs Rapidity and Coalesced Size Distribution: $y_{lab} > 0.5$. For the indicated rapidity cut, which corresponds to the E802 measurements, coalesced pairs for central collisions are almost uniquely from the s-i and i-i (mid-rapidity only) groups. In the limited events sampled here deuterons are also formed near projectile rapidities in peripheral collisions. The parentage of the successfully coalesced pairs is reflected in the average wave packet radii, significantly larger for central but somewhat above the $1fm$ value perhaps expected for peripheral.

Time–Rapidity Structure of Coalescence

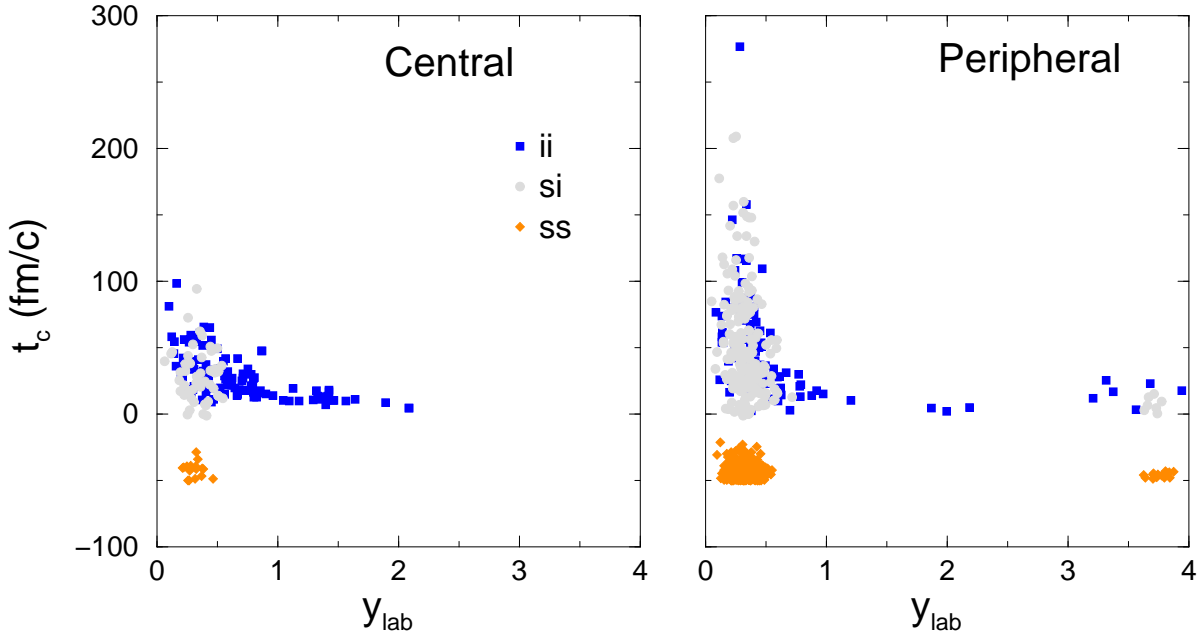


FIG. 15. Time-Rapidity Structure of Pairs. The time of coalescence t_c , i.e. the last interaction time for either nucleon, in the cascade global frame is plotted against rapidity for coalesced deuterons. Clearly in the global frame, i.e. the original equal velocity frame, the cascade follows interaction and coalescence for appreciable times. The s-s events, coming earlier and in a narrow time window, are easily distinguished, while the i-i events spread out appreciably in time.

Included as fig16.jpg

FIG. 16. Relative Momentum Window vs Rapidity. A most influential parameter for the success of deuteron formation is the momentum difference between the precursor nucleons. One notes the large values achieved for the totality of cascading s-i and i-i pairs, the very small values for all s-s, and contrasts these with the restrictive, ΔP , mostly less than 100 MeV/c, for the coalesced pairs. Small values of ΔP at coalescence follow from the low energy structure of the deuteron, and strongly influence the yields as functions of peripherality and rapidity. The matching of all pair ΔP 's to the deuteron wave function passes through the quantum filter in Eq. 7, and yields then reflect the overlap dynamics. There is a characteristic rise of ΔP with rapidity for the complete set of interacting pairs, signalling the increase in numbers of interactions towards mid-rapidity.

Included as fig17.jpg

FIG. 17. Relative Momentum vs Relative Separation. Coalesced deuterons are displayed in the lower two graphs, the central collisions to the right. ΔX , the np separation at coalescence is to be distinguished from the individual nucleon wave packet size. The coalescence window for this variable is defined by both the deuteron relative wave function and by the parentage group. The structure of the overlap factor in Eq. 7 contains a compensation from the Uncertainty Principle, but some model dependence in overall normalisation remains. The spread in ΔP for the spectator-spectator (intermediate shading) seen in this figure indicate the inclusion of Fermi motion for target and projectile nucleons.

Central Au+Au at 11.6 GeV/c

ARC-Dynamic Simulation: $b < 2$

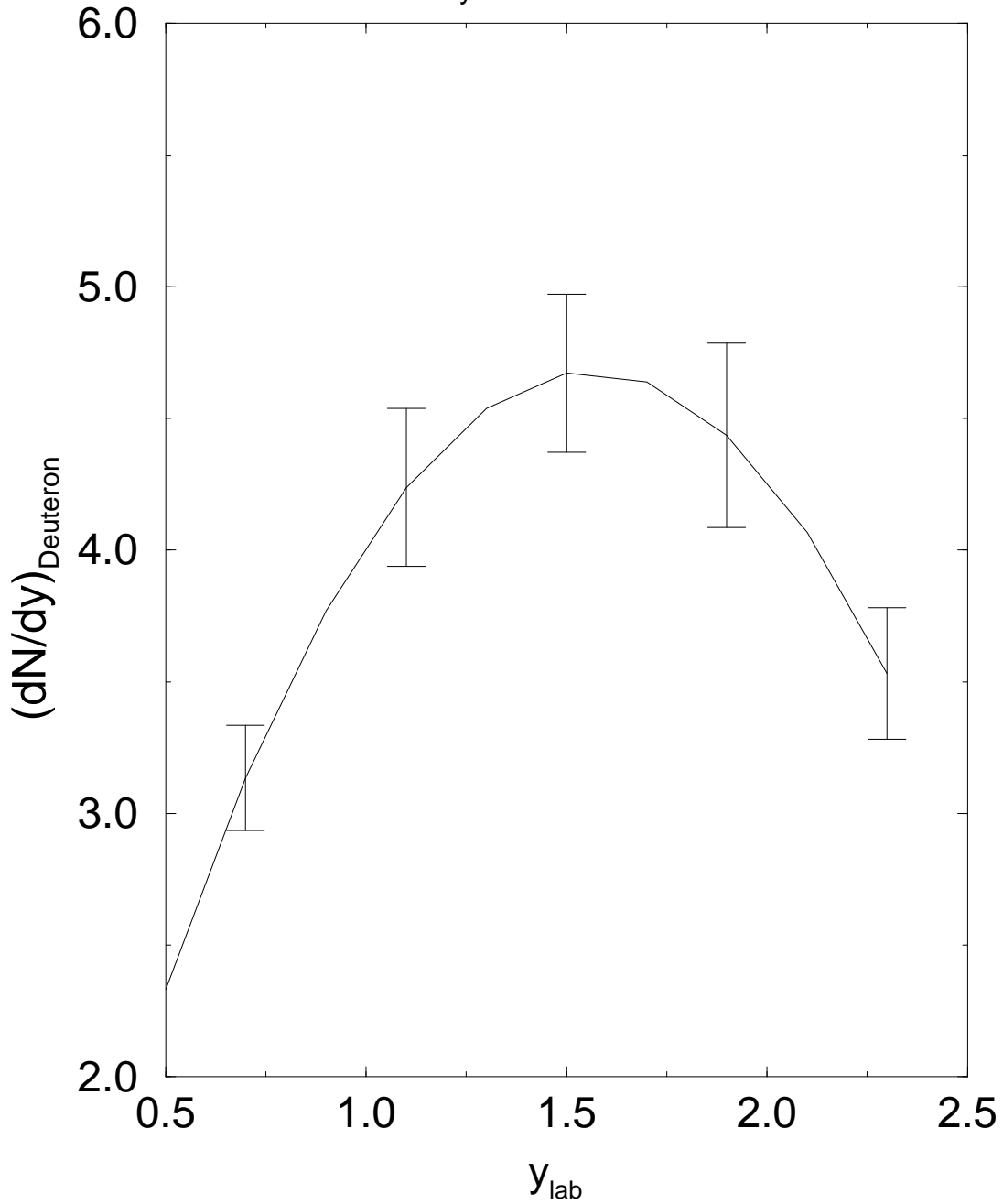


FIG. 18. Deuterons from ARC Dynamic simulation for Au+Au at 11.6 GeV/c. The centrality cut is defined simply by $b < 2$. Comparison with forthcoming data must incorporate the actual experimental trigger. The displayed curve was obtained by fitting a simple parabolic form to the theoretical data. The latter showed rather more fluctuation but contained statistical errors of about 10% as indicated.

$$\sigma^2 \sim \sum (x_i^2 - \langle x_i \rangle^2)$$

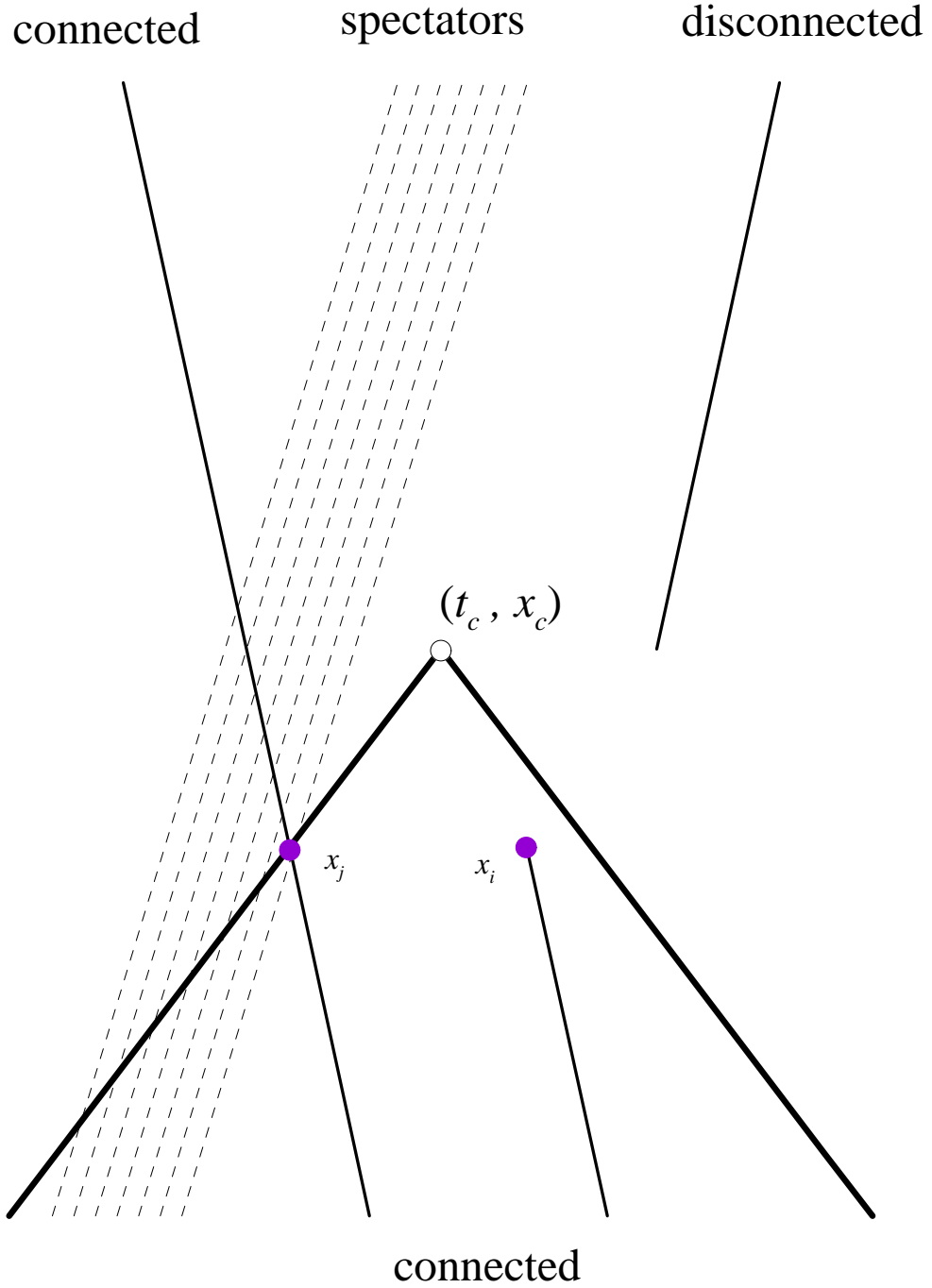


FIG. 19. Light-Cone Coalescence. A schematic of the space-time picture, at t_c , of particles which enter into the determination of wave packet size for the nucleon pair potentially forming a deuteron. The size parameter σ is obtained by averaging over the positions of all pair comovers, as defined in the text.

This figure "fig13.jpg" is available in "jpg" format from:

<http://arxiv.org/ps/nucl-th/9601019v1>

This figure "fig14.jpg" is available in "jpg" format from:

<http://arxiv.org/ps/nucl-th/9601019v1>

This figure "fig16.jpg" is available in "jpg" format from:

<http://arxiv.org/ps/nucl-th/9601019v1>

This figure "fig17.jpg" is available in "jpg" format from:

<http://arxiv.org/ps/nucl-th/9601019v1>